Neuroinformatics (2019) 17:5–25
https://doi.org/10.1007/s12021-018-9374-0

# New Features for Neuron Classification

Leonardo A. Hernández-Pérez[1] · Duniel Delgado-Castillo[1] · Rainer Martín-Pérez[1] · Rubén Orozco-Morales[2] · Juan V. Lorenzo-Ginori[3]

Published online: 28 April 2018


## Abstract

This paper addresses the problem of obtaining new neuron features capable of improving results of neuron classification. Most studies on neuron classification using morphological features have been based on Euclidean geometry. Here three one-dimensional (1D) time series are derived from the three-dimensional (3D) structure of neuron instead, and afterwards a spatial time series is finally constructed from which the features are calculated. Digitally reconstructed neurons were separated into control and pathological sets, which are related to three categories of alterations caused by epilepsy, Alzheimer's disease (long and local projections), and ischemia. These neuron sets were then subjected to supervised classification and the results were compared considering three sets of features: morphological, features obtained from the time series and a combination of both. The best results were obtained using features from the time series, which outperformed the classification using only morphological features, showing higher correct classification rates with differences of 5.15, 3.75, 5.33% for epilepsy and Alzheimer's disease (long and local projections) respectively. The morphological features were better for the ischemia set with a difference of 3.05%. Features like variance, Spearman auto-correlation, partial auto-correlation, mutual information, local minima and maxima, all related to the time series, exhibited the best performance. Also we compared different evaluators, among which ReliefF was the best ranked.

**Keywords** Neuron classification · Reconstructed neuron tree · Neuron features

## Introduction

A broad variety of applications and tools have been developed to study the neuronal tree-like structure, which are able to extract from it a large number of morphological features (Delgado Castillo et al. 2016; Scorcioni et al. 2008). The most widely used tool is the Sholl analysis (Sholl 1953), because it allows to obtain information about the complexity of dendritic branches on the neuronal trees. This is a very important point when it is necessary to compare sets of morphological structures having a high level of similarity. An example can be seen in (Mavroudis et al. 2014), where the morphological and morphometric variations were compared between neurons with Edinger-Westphal nuclei in Alzheimer's disease and normally aged neurons, concluding that they exhibit differences between their dendritic structures. Another example is the morphological analysis of the dendritic structure of pyramidal neurons from the cerebral cortex of the chimpanzee and its contrast to the cortex of the human brain. In the study of (Bianchi et al. 2012), the pyramidal neurons from the chimpanzee pre-frontal cortex showed a greater dendritic complexity compared with other cortical regions, which suggest that the evolution of cortical pre-frontal region in primates is characterized by a greater potential in regard to its connectivity for integration. Compared with chimpanzees, the human pyramidal neurons have a longer branching structure, with larger amount of branches in all the cortical regions. In the same way, the manner in which drugs influence the dendritic arborization has been studied

**Electronic supplementary material** The online version of this article (https://doi.org/10.1007/s12021-018-9374-0) contains supplementary material, which is available to authorized users.

✉ Leonardo A. Hernández-Pérez
leonardo.hernandez@etecsa.cu

[1] Empresa de Telecomunicaciones de Cuba S.A, Santa Clara, Villa Clara, Cuba

[2] Department of Automatics and Computational Systems, Universidad Central "Marta Abreu" de Las Villas, 54830 Santa Clara, Villa Clara, Cuba

[3] Informatics Research Center, Universidad Central "Marta Abreu" de Las Villas, 54830 Santa Clara, Villa Clara, Cuba

in (Leite-Morris et al. 2014), analyzing the reduction of these structures after the diminution of narcotic drugs, specifically morphine. On the other hand the neuron classification problem has been broadly addressed in the study of neuron sets by (Armañanzas and Ascoli 2015).

Recently published studies assert that the complexity of the brain, its hierarchical structure, as well as the sophisticated topological structure in which it organizes the neurons, are unexplainable in the neurosciences neither through the Euclidean geometry, nor using linear dynamics (Di Ieva et al. 2013, 2015) These references have been promoting the application of fractal analysis to quantify and describe the complicated dendritic structures. Fractal dynamics, as well as the fractal multi-scalar dimension (Schierwagen et al. 2007; Schierwagen et al. 2008), are perhaps the most used metrics to extract relevant information from morphological structures with a high level of complexity (Backes and Bruno 2012). The fractal theory has been used in neuron classification to establish the relationship between physiological and anatomical patterns (Fernández and Jelinek 2001), and has been also proposed in (Cross 1994; Dokukin et al. 2011) to study neural systems with high morphological complexity. A broad compilation of mathematical models from nonlinear dynamics, highly related with the neurosciences, is shown in (Saeb and Hövel 2013). An example of this would be the analysis of bifurcations through the Saddle-Node Infinite-PERiod (SNIPER) model, also known as the Saddle-Node on an Invariant Cycle (SNIC), or by the Fitz Hugh-Nagumo model.

The nonlinear dynamic analysis of time series is a powerful tool which has extended its application to many branches of scientific research (Papana and Kugiumtzis 2009). Topological equivalence is one of the main concepts that sustains theoretically the nonlinear dynamics procedures that have been implemented to characterize the discrete time series (Alligood et al. 2009; Rand and Young 1981). It is possible to investigate some important characteristics of an event using only the information contained in its associated time series. In particular, a dynamic multidimensional system can be described using the information obtained by measuring sequentially only one of its representative variables. Based on this concept, in this work we evaluated one-dimensional (1D) time series drawn from the three-dimensional (3D) neuronal structures, in order to obtain a new set of features that can be able to characterize these structures. The time series are obtained by analogy as the discrete sequences formed by successive coordinate increments in the branches of the neuronal tree. This approach opens the possibility to apply the time series analysis tools to obtain new features for neuron classification. Notice that the analysis tools employed in this study come from the time series theory and do not depend on the physical nature of the variable used in the abscissas. In the rest of this article, the sequences obtained as described above will be called time series.

Nonlinear dynamic analysis has been also used to study biological time series (Papana and Kugiumtzis 2009), combined with statistical methods. An example of this is the evaluation of mutual information using predictors such as: *k*-nearest neighbors (*k-NN*), equidistant and equally-probable predictors, as well as predictors based on the sum of correlations. Correlation estimation metrics and entropy have been used in the detection of dynamic changes. A broad collection of the above mentioned tools for the estimation of nonlinear metrics, used to measure complexity, dimension, and time series modeling, are implemented using the *MATS* tool (Kugiumtzis and Tsimpiris 2010).

In this work a novel way to analyze dendritic trees with high complexity is reported, using features obtained through splitting the 3D structure of the dendritic trees of traced neurons into time series. Here the reconstructed neurons are separated into control and pathological sets, both related to three categories of alterations caused respectively by ischemia, Alzheimer's disease (long and local projections), and epilepsy. Using the new features the classification results in terms of the correct classification rate (CCR) were improved in comparison to those obtained by using morphological features calculated by means of *L-measure* (Scorcioni et al. 2008). With the set of Alzheimer's disease (local and long projections) and epilepsy sets, these were 5.33, 3.75 and 5.15% respectively. The ischemic neurons did not have a better result. The above mentioned values correspond to the mean values of the all classification results from each dataset. In term of maximum values, these results were: 10.05, 11.63, 5.33 and 2.5% for: the ischemia, Alzheimer's disease (long and local projections), and epilepsy sets respectively. The features which most contributed to these results were: variance, Spearman auto-correlation, partial auto-correlation, mutual information and local minima and maxima. The top ranked evaluator was the ReliefF; whereas in the group of eight classifiers the best ones were *Logistic, MulticlassClassifier* and *Sequential Minimal Optimization (SMO)*, without significant statistical differences among them.

The rest of the paper is organized as follows: "Data and Methodology" section describes the sets of neurons used to extract the features and test the classifiers, the way in which the time series were built, how the features where obtained using *MATS* and *L-measure*, the tools used for feature computation, the methods for neuron classification and the evaluation of classifiers. The "Results" Section shows the classification results for each dataset, the best features within the whole set and the statistical analysis which validated the selected features, their evaluators, and the classifier algorithms. In the "Discussion" section we compare our results with others reported in unpublished works using the same sets of neurons. Finally the "Conclusions" section summarize the main results.

## Data and Methodology

### Selection of Neuron Sets

To calculate the new features proposed here and validate their effectiveness, we used some reconstructed neuron sets which included two or more subsets of data. Digitally reconstructed neurons are obtained by processing previously acquired image stacks (Halavi et al. 2012). In this case, neuronal trees are traced in 3D with dedicated computer-microscope interfaces or using specialized software. This allows the comparison of the results obtained in this work with others reported in the literature which use morphological features (Duan et al. 2003; Beguin et al. 2013; Dean et al. 2013).

The first set is available in (NeuroMorpho_Linkout 2018), with a total of 80 reconstructed pyramidal neurons from 11 monkeys of the genus Macaca. Among them, six are young *Macacafascicularis* monkeys, three male and two female, aged between 10 and 12 years, and one male, 12 years old *Macacamulatta*. The other five are two male and three female older *Macacamulatta* with ages between 24 and 25 years. The younger macaques have a corporal weight between 6 and 10 kg, whereas the older ones weigh between 4.5 and 10 kg. This set was partitioned into two subsets belonging to area 46 of the pre-frontal cortex. These two subsets are termed long- and local-projections. The long-projection comes from the upper pre-frontal cortex, whereas the local-projection corresponds to the inner pre-frontal cortex; having 43 and 37 neurons respectively. In the long-projection the neurons are divided again into two subsets: the first one with 19 neurons from the older monkeys and the second having 24 neurons form the younger ones. Similarly, in the local-projection the neurons are divided into 17 neurons from older monkeys and 20 from the younger ones. Issues concerning the surgical procedure, tissue preparation, and neuron reconstruction can be seen in (Kabaso et al. 2009; Duan et al. 2003; Duan et al. 2002). A second set of neurons used in this work was employed in (Beguin et al. 2013) and it has 40 reconstructed pyramidal neurons from rat hippocampus. From them, 20 were taken from wild rats and 20 from rats genetically modified by enlarging the polyalanine of the aristaless-related homeobox (ARX) gene. This mutation is usually found in the West and Ohtahara syndrome (Absoud et al. 2010). Additional information about the rats used and the neuron tracing procedures followed can be found also in this reference. A third set of neurons was also used in this work, which is referenced by (Dean et al. 2013), with 200 pyramidal neurons from the infra- and supra-granule neurons in the neocortical layers of the frontal region. From these, 100 belonged to the ischemia group. All of them were obtained from 8 sheep fetuses between 120 and 126 days of gestation. The control group was obtained from 4 of the fetuses and from the other 4 the ischemia group. The reconstructed neurons were classified according to their location: from the infra-granule layer, 51 control cells and 48 ischemic cells; whereas from the supra-granule layer, 49 control cells and 52 ischemic cells. Their reconstruction is available in (Ascoli et al. 2007), and the methods used to acquire them are explained in (Dean et al. 2013; Riddle et al. 2006, 2011).

### Chaos Test

The test used to verify that the series we are dealing with are chaotic was introduced by (Gottwald and Melbourne 2009). It was applied to a group of neurons drawn from each one of the sets, previously to the beginning of this research. We recognize that if the result of this test were not successful there would not be a reliable mathematical foundation to sustain the existence of a homomorphism between the three dimensional structure of the neuron and one of the representative variables, in this case the one-dimensional series corresponding to each neuron coordinate. This test is not intended to form a part of the algorithm proposed in this study to obtain features from the time series. We assume instead, that each of these series comply with this condition given the high degree of complexity of the three-dimensional neural structures and the results of the tests previously performed with each of the data sets.

In the paper from Gottwald and Melbourne cited above, a new test for chaos was introduced. The input to it is any time series that may come from a discrete map, a differential equation or an experiment. The output is a single number, which in theory is either 0, for non-chaotic data, or 1, for chaotic data. In practice, the result is close to 0 or close to 1, provided that enough data is used and that the input data is not over-sampled. The test has some advantages over other methods such as calculating Lyapunov exponents.

Z1TEST, Matlab function (*0–1 test for chaos - File Exchange - MATLAB Central* 2018), implements the 0–1 test as described in their most recent paper, "On the Implementation of the 0–1 Test for Chaos" (Gottwald and Melbourne 2016). This method to detect chaos is applied directly to the time series data and does not require reconstruction of the phase space. Moreover, the dimension and origin of the dynamical system are irrelevant. The input is the time series data and the output is zero or one depending on whether the dynamics is non-chaotic or chaotic.

This test was applied to each one of the time series used in this study and the result was that all the series are highly chaotic. Most of the tools that are used to determine chaos in a time series are based in calculating the Lyapunov's exponent (Rosenstein et al. 1993). The most referenced tool of this kind is probably Chaos Data Analyzer (CDA), (Chaos and Time-Series Analysis, 2018; Hamilton and West 2000). Other tools

like (TISEAN: Nonlinear Time Series Analysis, 2018; BenSaïda 2015) appeared recently. All the mentioned tools were used in this research to test the presence of chaos in the time series that were analyzed.

## Time Series Construction

The 3D structure of the reconstructed neuronal tree can be decomposed into time series from the coordinate system values of each point in the morphological structure of the tree. Figure 1 shows the projection in the *XY* plane of a 3D reconstructed neuron.

In Trees Toolbox (Cuntz et al. 2011) three ordering methods are proposed: hierarchical, topological and lexicographical. There is need to have a unique ordering to compare trees. The topological ordering was used along all this work, after verifying experimentally that it led to better results than the other orderings. Topological ordering sorts the indexes by considering the path lengths and the levels' orders, which results in a unique equivalence relationship.

The index ordering that each node of the neural tree possesses will determine the order of the points in the 1D sequence. In our study the topological ordering (Cuntz et al. 2011) was used. In both types of sequences (with and without jumps) the order of each node's indexes was followed. Figure 1 shows an example using the neuron P18-DEV340, starting from branch 6 (node 1 in the figure) and Fig. 2 shows the coordinate series with jumps (*CS-WJ*) 1D corresponding to the *Y* coordinate. This sequence is formed by means of subtracting, from each node, the respective coordinate value (*X*, *Y* or *Z*) of its father (previous) node. When a termination is reached, a jump occurs. The example in Fig. 1 begins by node 1 following consecutively the nodes in the right branch until reaching termination 13, continues in node 14 until termination 19 and similarly from node 20 until termination 28 and finally terminations 29 and 30. At the end of a branch in the sequences with jumps, the coordinate values of the previous node are subtracted from that of the current node (e.g. X20 – X19). In the sequences without jumps the coordinate value of the father (previous) which will always be a bifurcation node is subtracted from the current (son) node (e.g. X20 –X2).

The time series obtained, whose values are the coordinates between each point in the tree, are transformed into a series of intervals in a way analogous to that used to obtain the tachograms in heart rate variability studies (Task Force of the European Society of Cardiology and the North American Society of Pacing and Electrophysiology 1996). In this, the ordinates are the differences between consecutive points as shown in Eq. (1).

$$X_n = (X_1 - X_0); (X_2 - X_1); \ldots; (X_n - X_{n-1}) \quad (1)$$

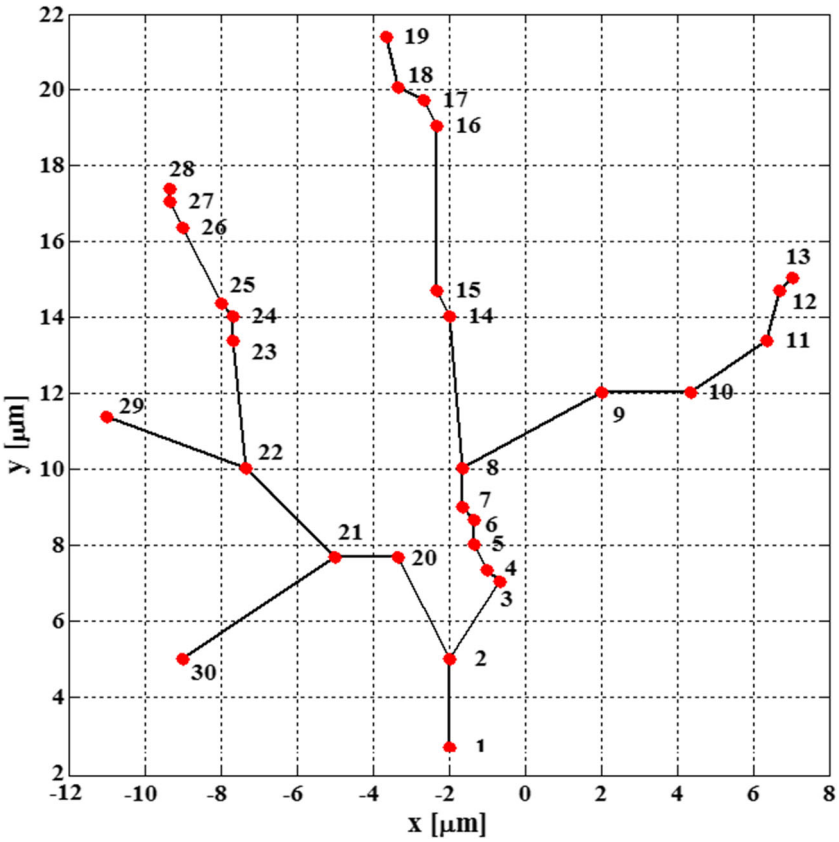


**Fig. 1** Topological ordering of the neural tree, projection on the XY plane. When a termination is reached, a jump occurs. The example in Fig. 1 begins by node 1 following consecutively the nodes in the right branch until reaching termination 13, continues in node 14 until termination 19 and similarly from node 20 until termination 28 and finally terminations 29 and 30. At the end of a branch in the sequences with jumps, the coordinate values of the next node are subtracted (e.g. *X20 – X19*). In the sequences without jumps, the coordinate value of the father node, which will always be a bifurcation (e.g. *X20 –X2*), is subtracted from the current node's coordinate. See in Fig. 2 the coordinate series with jumps (*CS-WJ*) corresponding to the *Y* coordinate. This sequence is formed by means of subtracting the respective father node coordinate value (*X, Y or Z*) from the son node coordinate for each node

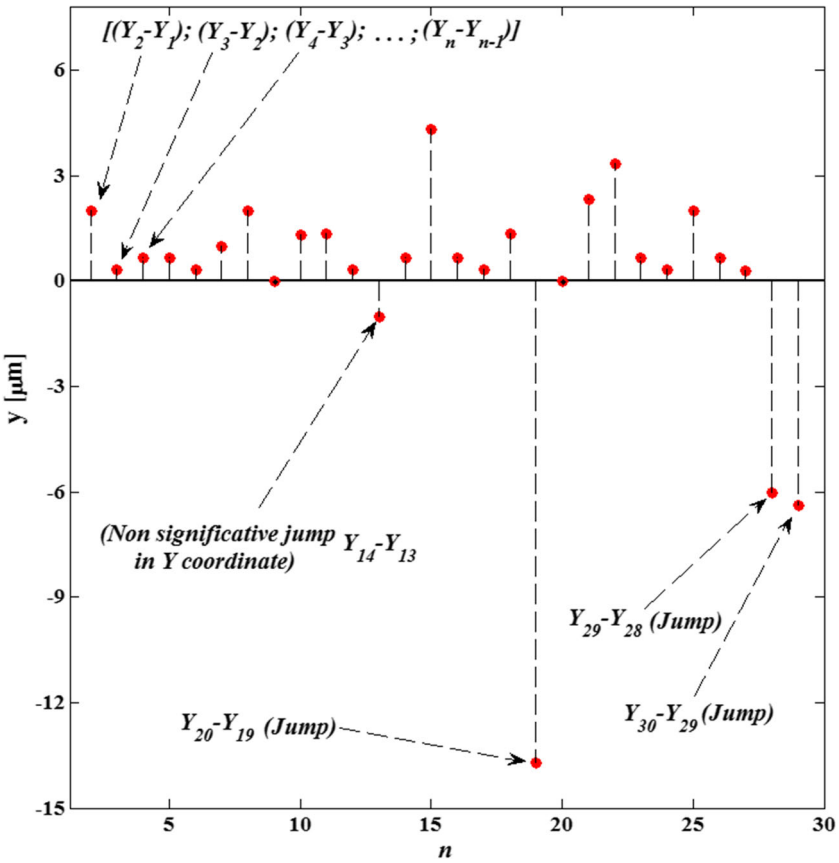


**Fig. 2** Coordinate series with jumps (*CS-WJ*) corresponding to the *Y* coordinate. This sequence is formed by means of subtracting the respective coordinate value (*X*, *Y* or *Z*) from the previous nodes (termination) from that of the current node in the new branch. In $n = 13$ a small jump occurs due to the small difference existing between $Y_{14}$ and $Y_{13}$ (14.05 and 15.06 μm respectively). On the other hand, in $n = 19$ ($Y_{20}$- $Y_{19} = -13.71$ $\mu m$) a significant jump occurs

There are some methods which can be used to represent the 3D structure in planes. The neuron tracing tools and algorithms employed in (Zhou et al. 2016; Vasilkoski and Stepanyants 2009) make use of the maximum intensity projection method described in (Wallis and Miller 1991), in which the *XY* plane corresponds to the maximum intensity projections, and then the other planes (*XZ*, and *YZ*) are related with this. This method ensures a unique relationship between the coordinate system and the neuron related to it. It is also usual to use only the plane of maximum projected intensity to analyze 3D structures, which leads to a loss of information about the 3D structure. This novel procedure to analyze the dendritic structure is based in the concept of topological equivalency described in (Rand and Young 1981; Alligood et al. 2009), which proves that it is possible to investigate important characteristics of a multi-dimensional dynamic arrangement using only the information from a one-dimensional time series obtained from it.

Topological equivalence (homomorphism) is one of the primary concepts that lie beneath as theoretical support in all the procedures that were implemented on the basis of nonlinear dynamics theory, to characterize discrete time series. The starting point here is a one-dimensional time series $\{X[n]\}$ where $n$ is the time index of the sequence originally obtained through sequential sampling of a continuous variable.

The Takens embedding theorem (Rand and Young 1981) states that with the knowledge about a system's representative variable in the form of a numerical sequence, it is possible to obtain information on the geometry, dynamics and topology of this system.

In our case, $x(t)$ is the organized sequence of dendrites as continuous element from which the discrete time series $\{X[n]\}$ (which is actually a series of spatial intervals, according to the convention adopted) composed by the $n$ values obtained from the digital tracing of the neuron.

In spite that it is not our interest to study the neuron as a dynamical system to analyze its evolution, the above-mentioned theorem is used as the basis to obtain a wide set of features which allow obtaining information on the topology of this system.

To apply the Takens' embedding theorem it is necessary to apply two fundamental tests: (1) show that the series obtained are chaotic and (2) reconstruct the attractor from the information obtained from one of its time series. The attractor reconstruction was made applying the embedding method, starting from calculating the embedding dimension ($n$) and the time delay ($\tau$).

In summary, the neuron is considered as a dynamical system with multiple variables, from which the coordinates of each one of its elements are known (bifurcations,

continuations and terminations [BCT]) that conform the 3D structure of this system. Each one of the series of coordinates has a topological ordering described in (Cuntz et al. 2011). These series of coordinates are transformed into series of intervals, analogously to the construction of the tachograms used to study the heart rate variability as mentioned previously. This transformation allows representing in the ordinate axis the values of the distance components between successive elements [BCT] which compose the 3D structure of the neuron, when every point is projected into the coordinate axis as shown in Fig. 2, the abscissas being the ordering number.

The time series were obtained from the coordinates of the neuronal tree elements, properly arranged and transformed as series of intervals.

The above explanation of the transformation from time series to series of intervals did not take into account that each node in the neuronal tree is associated with a previous ('father') node, excepting the root node. This procedure generates jumps in the obtained series of intervals whenever the preceding node is a tree ending point. As example, the node number 20 in Fig. 1, has been ordered after the ending node number 19. This is the cause of the jump observed in Fig. 2 between the nodes 19 and 20. In subsequent paragraphs we will refer to this as coordinate series with jumps (*CS-WJ*). To understand how the jump series were constructed see the animation (Online Resource 1).

Another way to obtain the series of intervals is considering the nodes parent-child relationship to prevent the previously mentioned jumps. Thus, reconsidering the previous case of Fig. 1, it is necessary to subtract the coordinates of parent node (which is for example node number 2) from those of node number 20.

Using this procedure is obtained the coordinate series without jumps (*CS-WOJ*). From each reconstructed neuronal tree we obtain three series following the above mentioned procedures.

To reduce the dimensionality and to obtain a single series with the morphological information from the 3D neuron representation, we calculated the $L_2$-*norm* for each spatial point from the corresponding series of intervals using Eq. (2).

$$S_n = \sqrt{(X_n - X_{n-1})^2 + (Y_n - Y_{n-1})^2 + (Z_n - Z_{n-1})^2} \qquad (2)$$

Equation (2) is calculated for all the neuronal tree points, $n$, to obtain a morphological representation of the neuron in function of the spatial location of the tree node coordinates. Values of $S_n$ are calculated traveling from the lowest level (starting node) to the highest levels.

Four groups of series are obtained for each neuron set. These four groups of time series are termed as: coordinates' series with jumps (*CS-WJ*) and without jumps (*CS-WOJ*), and spatial series with jumps *(SS-WJ)* and without jumps (*SS-WOJ*). Note that we are terming as a neuron set the collection of traced neurons, while the term group is used to designate the collection of time series obtained from each neuron set. In this way, for each neuron, three coordinate series and a single spatial series are obtained.

In our study coordinates *X*, *Y* and *Z* were selected given that each of them can provide information about the system from which they come (the 3D neuron), following the principle of Takens' theorem. After this, a series of intervals is obtained from each coordinate as explained before. These series of intervals provide information about: dimension of the elements composing that coordinate, total dimension of the neuron in this coordinate as well as others that have been mentioned above like: number of terminations, lengths of the branches and associated to the latter the amplitude of jumps. We considered at the beginning that integrating the coordinate series in a spatial one would lead to at least similar results while it would also reduce the dimensionality of the data set. However, the results revealed that obtaining the spatial series from the information of each coordinate implies a significant loss of information. We observed that using together all the diversity of features in each of the interval series corresponding to the coordinates allows a better characterization of the neuron's 3D structure. We consider that information loss in the spatial series is due to the fact that integrating the coordinates through the *L2* norm suppresses information on the true extension of the neurons' morphology.

## Additional Information About the Construction of Time Series from Neuron Trees

Within the research stage of this study, we conceived the analysis of each one of the series that can be obtained from the possible paths within the dendritic structures.

We analyzed firstly the possibility of using the path from each node until the root and consider it as a time series. After this we obtained the corresponding series of intervals. With this method, a number of time series as large as the number of nodes (neuron segments) can be obtained. However, notice that this method would lead to a large amount of small series that are useless in regard to applying time series analysis tools.

A better method would be to consider only the paths that follow the tree from the root to each termination. Using this method the number of time series is reduced significantly and a good morphological description of the neuron tree is made. This procedure would also guarantee working with time series of adequate length.

In both cases we have considered that it is more convenient to unify appropriately the series obtained in a unique one and afterwards to extract the features from them. Another possibility would be to work with the set of series and build a dataset with all the features obtained

for each series. We consider that this could be useful to search for differences among groups but at the expense of a very high computational cost.

## Feature Extraction

Using the *MATS* tool (Kugiumtzis and Tsimpiris 2010), a dataset of metrics was extracted from each one of the four previously obtained series. Three kinds of metrics are originated by *MATS*: linear, nonlinear, and others. Nonlinear metrics contain a group of correlation, dimension and complexity metrics, as well as modeling metrics. From these groups we obtained: Pearson autocorrelation, bi-correlation, cumulative bi-correlation, mutual information, dimension of correlation, Hurst exponent and others. Some of these metrics are parameter-dependent, as time delay adjustment for correlation analysis, or the embedding dimension for the dimension of correlation. In this work we investigated a total of 175 metrics (a complete relation is shown in Appendix 1 (Online Resource 2) obtained from each one of the four created series, with a total of 525 features for each series, plus 175 features for spatial series on every reconstructed neuron in each set.

## Morphological Features

To compare the aforementioned metrics, we made use of the morphometric features obtainable by the *L-measure* software (Scorcioni et al. 2008). This tool allows obtaining the minimum, mean, and maximum values, as well as the total sum and the standard deviation, of 44 different metrics related to morphological features, which make in total $5 \times 44 = 220$ metrics. For some features, these parameters are obtained with repeated values or are without interest for the morphological analysis of the neuronal trees. After an analysis of each one of the 220 metrics, we select 81 of them as those having significance for this study; see Appendix 2 (Online Resource 3).

These 81 metrics were selected taking into account the *L-measure* recommendations for each function, like for example "*Total_Sum of the Pk_classic function does not make sense*". Metrics with equal mean, minimum, maximum, and total sum values were taken as a single metric. For example, calculating the neuron surface only the value of the total sum is useful, because the values: minimum, medium and maximum have the same value as the total sum, and the standard deviation equals zero.

According to the four groups of series described in section 2.2, the extracted features were termed: dataset of coordinate series with jumps *(CS-WJ),* dataset of coordinate series without jumps *(CS-WOJ)*, datasets of spatial series with jumps *(SS-WJ)* and dataset of spatial series without jumps *(SS-WOJ)*. Moreover, a morphological dataset was obtained, which is termed *(MORPHO)*.

## Feature Selection and Classification

We made use of the *Weka* tool (Bouckaert et al. 2015) to select the features employed and to evaluate their effectiveness during classification of neurons. A first exploratory trial was performed in order to make an estimation of the recommended classifiers for each dataset of features. For this, a selection procedure using various low computational cost evaluators was implemented for each dataset of features. All the evaluators used a ranker type searching algorithm, these were, according to the *Weka* terminology (Bouckaert et al. 2015): *ChiSquaredAttributeEval*, *FilteredAttributeEval*, *GainRatioAttributeEval*, *InfoGainAttributeEval*, *ReliefFAttributeEval*, *SVMAttributeEval*, and *SymmetricalUncertAttributeEval*.

The 52 *Weka* classifiers that were employed were: three characterized as Bayesian (*BayesNet*, *NaiveBayes*, and *NaiveBayesUpdateable*), six categorized as "*functions*" (*Logistic*, *RBFNetwork*, *SimpleLogistic*, *SMO*, *SPegasos*, and *VotedPerceptron*), three considered as "*lazy*" (*LWL*, *IB1*, and *IBk*), thirteen catalogued as "*meta*" classifiers (*Bagging*, *Dagging*, *Decorate*, *ClassificationViaClustering*, *ClassificationViaRegression*, *CVParameterSelection*, *END*, *FilteredClassifier*, *Grading*, *LogitBoost*, *MultiBoostAB*, *MultiClassClassifier*, and *MultiScheme*), four classifiers from the set named "*mi*" (*ClassificationViaRegression*, *MISMO*, *MIWrapper*, and *SimpleMI*), two in the "*misc*"group (*HyperPipes*and*VFI*), eight "*based-on-rules*" classifiers (*ZeroR*, *ConjunctiveRule*, *DecisionTable*, *JRip*, *NNge*, *PART*, *Ridor*, and *OneR*), and thirteen "*decision-tree*" classifiers (*J48*, *ADTree*, *BFTree*, *DecisionStump*, *FT*, *J48graft*, *LADTree*, *LMT*, *NBTree*, *RandomForest*, *RandomTree*, *REPTree*, and *SimpleCart*). We excluded in the exploratory trials the classifiers based on artificial neural nets because of their higher computational cost. The rest of the classifiers implemented in *Weka* (not mentioned earlier) failed to classify at least one of the datasets and were excluded in this study, given that the purpose was to apply the same classifiers to all sets.

The recursive attribute selection process was performed using all the default *Weka* values (Bouckaert et al. 2015), both for a 10-fold cross-validation and using a random seed as well. A more recent study (Armañanzas and Ascoli 2015) makes a wide revision of the state of the art of neuron classification and highlights cross-validation (10-fold) as one of the most used methods. The number of classifications in a dataset will depend upon the number of features. Table 5 shows an example of the recursive feature selection and classification process, for a specific evaluator-classifier combination and a dataset having 81 features. The whole process to classify a dataset generates 364 tables of this kind, each one with 7 classifications which produces 2548 results. From these results, only those corresponding to a 10:1 features – instances ratio were

selected, according to the criteria from (Foster et al. 2014) to avoid overfitting of the classifier due to an excess of features. If we consider that the set under analysis includes 40 instances in total (TNI), only the classifications having four features or less comply with the 10:1 ratio and these add up to 1092 classifications out of 2548. The other 1496 classifications are not considered because these don't satisfy the 10:1 ratio criterion. For example, classifying 40 instances using 10 features does not exclude the possibility of overfitting.

Given the large number of features extracted from the sets of neurons, and according to (Foster et al. 2014), a recursive procedure was implemented to eliminate approximately one half of them in every iteration, in order to have approximately one feature for every ten instances having in mind to have at least 10 instances per feature. For example, a dataset with 40 instances and 81 features needs seven recursive cycles to obtain 41, 21, 11, 6, 4, 3, and 2 features. In each of the feature selection cycles a classification was performed, but only the classification results with 4, 3, and 2 features are taken into account to keep an acceptable instance-to-feature ratio.

The recursive method to select features is independent of the classification, even though these were performed simultaneously. This is valid if a ranker type search algorithm is used, which returns the features or part of them organized decreasingly according to their importance. To demonstrate the independence between data selection and classification, a data set of cardinality 525 was employed, from which features were selected successively until reaching the numbers 256, 128, 64, 32, 16, 8, 6, 4, 3 and 2. With each set a new independent dataset was created and afterwards each one of them was classified independently. The results were the same by both ways, which allowed verifying that the ranking method is independent of the classification algorithm.

On the other hand, one of the objectives of this work was to explore as much features obtained from the time series as possible, to find those that provide valuable information about the 3D structure of the neuron. Being able to discriminate among a larger set of features helps to find those having the best performance and consequently to improve neuron classification through morphological features.

Table 5 in the "Results" section shows the morphological features of an epilepsy set obtained using the *SVMAttributeEval* evaluator with the ranker searching algorithm, and a logistic classifier.

To determine which dataset of features showed the best performance, we built two new datasets taking the best 15 ranked features from each dataset: the first one, with the features obtained from each dataset of series (*CS-WJ*, *CS-WOJ*, *SS-WJ*, and *SS-WOJ*) totaling 60 features, and the second one adding to the first group the 15 best morphological features obtained from *L-measure*. To select the best 15 ranked features we implemented a recursive process of feature selection and classification using the *SVM* evaluator. This made use of the *Weka*'s ranker searching algorithm, which reduced iteratively the amount of features to 50, 30, and finally to 15.

Seven datasets were obtained in total for each neurons' set, as depicted in Fig. 3: two datasets with 525 features (*CS-WJ* and *CS-WOJ*), two with 175 features (*SS-WJ* and *SS-WOJ*), a dataset with 60 features (the top 15 of the four previously mentioned dataset, termed *U-SERIES*), a dataset with 75 features termed *U-MORPHO* that contained the above described *U-SERIES* plus the top 15 of the dataset of morphological features), and finally the morphological dataset which contains 81features (*MORPHO*).

## An Alternative Method: Training and Test

Another, more reliable procedure to make an appropriate attribute selection and classification was also implemented following (Pawel et al. 2009), which divides the dataset in two subsets for training and test. This procedure is more effective to prevent overfitting of the classifiers and was applied to compare its results with those previously obtained using k-fold cross-validation. The results applying this method to the epilepsy dataset are shown below. This method, as well as the previously implemented one, takes into account the classification results when the instances/features ratio 10:1 is fulfilled (Foster et al. 2014). The differences are the following:

1. The datasets were divided in training and test subsets in the proportion 2/3:1/3.
2. The four best features were selected from the train set and used to train the model.
3. The test subset was classified with the trained model.

## Statistical Analysis

All statistical comparisons between groups were performed using a Student's *t*-test for independent samples in the cases where the variables have a normal probability distribution and a Wilcoxon rank-sum test for independent samples, if any variable was not normally distributed.

Multiple comparisons were evaluated using the Friedman test, given that the assumption that the variables were normally distributed did not hold in all cases.

## General Procedure

The system implemented to obtain and select the neuron features and to evaluate their success when used in neuron classification can be summarized by means of the block diagram shown in Fig. 3. The procedure depicted was applied to each neuron set and its results will be analyzed in the next section.

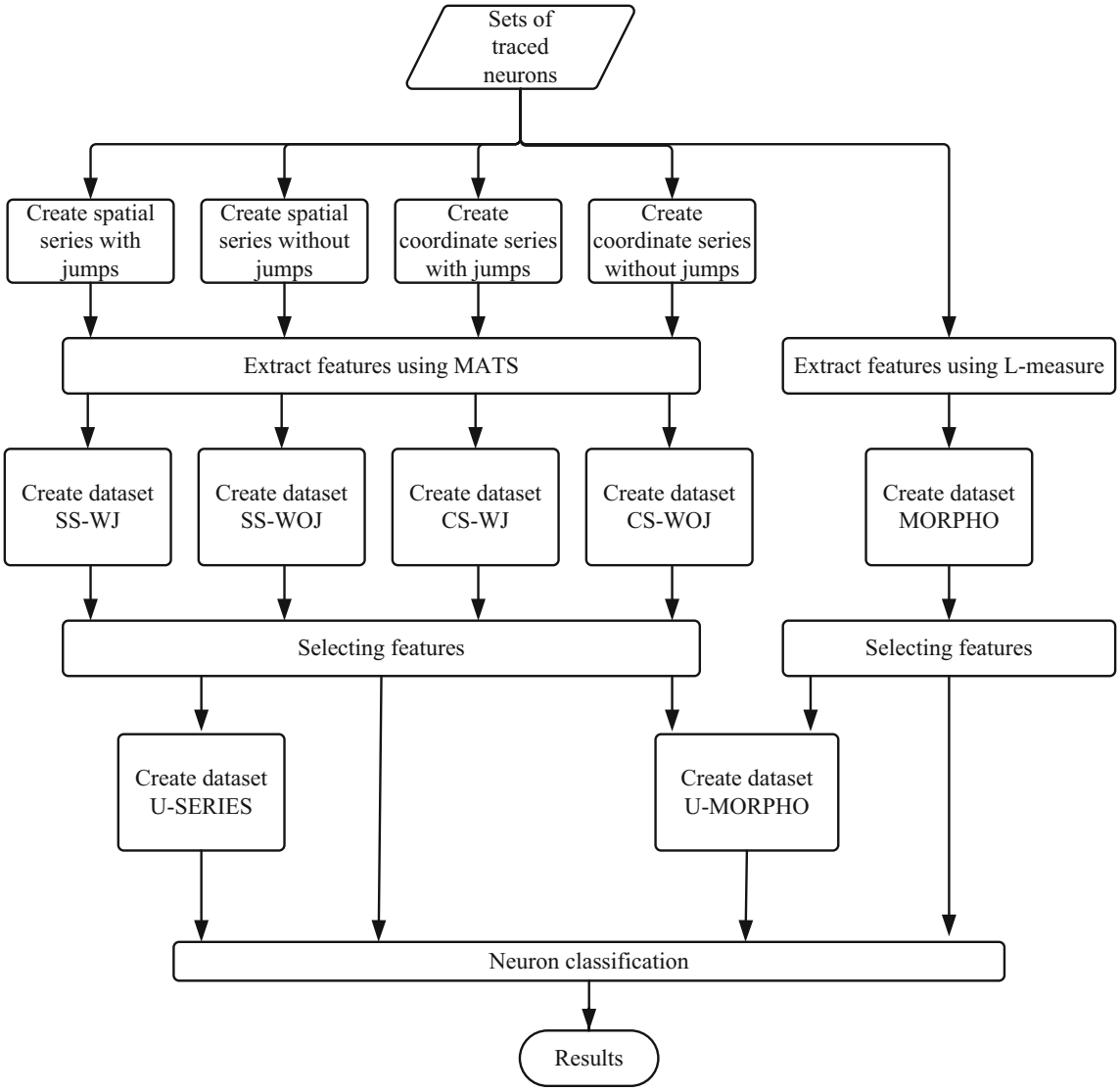


**Fig. 3** Block diagram of the method implemented to select neuron features and to evaluate their success in classification. A comprehensive workflow and all the required scripts to reproduce the results can be obtained in https://github.com/leonardo-hernandez/New-features-for-neuron-classification/

The block diagram has as input the neurons sets from which the time series were extracted. These series were introduced in *MATS* to obtain the features. With these features, the datasets were constructed afterwards and the recursive procedures for feature selection and classification were applied. The results of this classification were tabulated in descending order, thus obtaining the best 20 classifications together with their respective features.

## On the Interpretation of Results

Interpretation of results should be made carefully due to the large number of classifications performed. Taking into account the whole set of classifications, these results can lead to misinterpretation errors, which are related in first place to the features involved in the results. Table 2 in the "Results" section shows a summary of the best features obtained from the 20 best classifications, considering the rate with which a given feature appears in first, second or third position. However, if we analyze the whole set of results, the best features obtained were not the same while the reader could think that similar results were obtained with these features, which was not the case.

Something similar occurs with the results pertaining to the comparison among evaluators. For the 20 best results, the SVM evaluator showed significant differences when compared to the rest of the evaluators with the exception of ChiSquared. These two evaluators have a higher performance than the ReliefF evaluator if we only consider the 20 best classifications. However, ReliefF had the best performance when all the classifications were taken into account, which could lead to another erroneous interpretation.

Making a similar analysis for the classifiers, this situation repeats again. The *FT* classifier had the best performance for the 20 best classifications, but ranks the seventh in importance when all the classifications are taken into account. Another issue is that there is no coincidence in the order of importance of the classifiers when comparing the 20 best classifications within all the classifications. The reader interested in reproducing the procedure proposed in our paper, could think that the best result were obtained always using the *FT* classifier which was not the case.

Other issues are the box plots and multiple comparisons among datasets. Both graphs are included using the results from all comparisons due to the fact that there are not large differences compared to the results of the 20 best comparisons. However the authors wish to point out that these differences are noticeable for the ischemia set.

## Results

The results of this research are presented in the same order that was used in the previous section. Firstly we analyze the chaos test result, followed by the quantitative results of feature selection, taking into account the four datasets based on series, the union of these features, and the union of the features from series and from *L-measure*. Next, the analyses of the classification for each dataset are presented. Additionally, an analysis of the best evaluators and classifiers is included. The results for classifiers which showed low effectiveness should not be considered, neither to determine the best features nor to compare the datasets, given that this could lead to interpretation errors due to reasons like those explained earlier in the section "On the interpretation of results". However, to compare the effectiveness of classifiers and evaluators we do consider appropriate to take the whole results.

In the "Classification" section we took into account all the classification results. The 20 best results can be seen in the Online Resource 5.

This study aimed to include as much classifiers and evaluators as possible because there are not previous references on neuron classification using features of this nature. We took the 20 best classifications with the purpose of selecting the set of features, evaluators and classifiers that showed the best performance.

### Chaos Test Results

To make appropriate tests to verify whether the time series exhibit chaotic behavior or not, the computational tools Z1TEST (Gottwald and Melbourne 2009), CHAOSTEST (BenSaïda 2015), CDA-LE (Chaos and Time-Series Analysis, 2018; Hamilton and West 2000) and TISEAN (TISEAN: Nonlinear Time Series Analysis 2018) were employed. The Z1TEST chaos test was applied to the whole datasets of time series extracted from the neuron's tree. This step was performed previously to the procedure described in Fig. 3. Table 1 shows an example of the results, while the whole results can be seen in the Online Resource 6. The possible values obtained from Z1TEST are between zero and one, where values near one mean the presence of chaos. In the rest of the results the chaos measure took values between −1 and 1, in which values higher than zero indicate the presence of chaos. Almost the totality of results showed the presence of chaos in the time series obtained from the decomposition of neuron trees. Another alternative used was CHAOSTEST, which showed different results. In the case of spatial series, none of them showed the presence of chaos. This result suggests that the transformation applied ($L_2$-*norm*) to obtain this kind of time series, might have reduced or suppressed its chaotic behavior. The absence of chaos is consistent with the poor results obtained in the classification of neurons using chaos-related features obtained from these time series.

### Best Result Using Features from Series

Taking only ten instances by feature, Table 2 shows the ranking of the best features for each series. As an example, in the spatial with jumps series the feature *LocalMinimSDa1w1* was number 1 in the ranking, because it was the best positioned 22 times. The features of the coordinate series with and without jumps are ended in *_X*, *_Y*, or *_Z*, indicating the coordinate from which they came. To obtain the results shown in Table 2, 560 classifications were selected corresponding to the best 20 results for 28 datasets from four sets of neurons (seven datasets for each one).

### Results Using the Union of Features Dataset from Series

Table 3 shows the comparison of best performance features, in the classification of the union of series dataset of features (*U-SERIES*). It can be observed that 7 out of the 10 features belong to the series of coordinates, in which 5 of them correspond to the series of coordinates with jumps dataset (*CS-WJ*). Half of the features correspond to the "*Y*" coordinate. These results suggest that, in this study, the series of coordinates showed a better performance compared to the spatial series.

If we consider that jumps occur only in each termination, each time series will have as much jumps as terminations, which is itself an element of the neuron's morphology. This will be reflected in the with-jumps coordinate series (*CS-WJ*) and can allow a better differentiation of the corresponding

**Table 1** An example which shows in the first column the type of reconstructed series for the *CS-WJ* case, in the second column the series' name, the third column shows the results for the 0–1 test for chaos, implemented through the Matlab function Z1TEST; the fourth column shows the results obtained using the function CHAOSTEST, which estimates the value of the Lyapunov's exponent to detect the presence of chaos

| Time Series | Series Name | Z1TEST | CHAOS TEST | CDA-LE | Lyap_k | Lyap_r (D1 M2) | Lyap_r (D1 M3) | Lyap_r (D2 M2) |
|---|---|---|---|---|---|---|---|---|
| CS-WJ | X_Group1_Serie1.dat | 0,9983 | 0,0227 | 0,2309 | 0,0050 | 0,0047 | 0,0062 | 0,0045 |
| CS-WJ | X_Group1_Serie10.dat | 0,9984 | 0,2105 | 0,2308 | 0,0061 | 0,0036 | 0,0042 | 0,0035 |
| CS-WJ | X_Group1_Serie11.dat | 0,9983 | −0,1534 | 0,2057 | 0,0052 | 0,0043 | 0,0059 | 0,0045 |
| CS-WJ | X_Group1_Serie12.dat | 0,9985 | 0,1035 | 0,2881 | 0,0054 | 0,0045 | 0,0058 | 0,0044 |
| CS-WJ | X_Group1_Serie13.dat | 0,9978 | −0,0746 | 0,2520 | 0,0047 | 0,0057 | 0,0067 | 0,0060 |
| CS-WJ | X_Group1_Serie14.dat | 0,9982 | −0,0067 | 0,2197 | 0,0041 | 0,0037 | 0,0050 | 0,0037 |
| CS-WJ | X_Group1_Serie15.dat | 0,9972 | −0,2890 | 0,3130 | −0,0037 | 0,0027 | 0,0026 | 0,0028 |
| CS-WJ | X_Group1_Serie16.dat | 0,9983 | 0,0351 | 0,2941 | 0,0024 | 0,0042 | 0,0049 | 0,0042 |
| CS-WJ | X_Group1_Serie17.dat | 0,9987 | 0,0587 | 0,1795 | 0,0047 | 0,0045 | 0,0061 | 0,0042 |

Using a similar method, column 5 (CDA-LE) shows the results of the Lyapunov's exponent obtained by means of Chaos Data Analyzer (CDA, professional version). Columns 6 to 9 exhibit the results obtained using the functions lyap k and lyap r of TISEAN. In column 6 these are for lyap k with the default values and the rest of the columns correspond to lyap r with various time delays (D) and embedding dimensions (M). For example lyap r (D2 M2) indicates that the result was obtained with D = 2 and M = 2

neurons. Another element will be the jump amplitude, which will be larger in neurons with more elongated branches. Both previously mentioned elements are not present in the coordinate series without jumps (*CS-WOJ*) and for this reason we understand that the coordinate series with jumps contain more information about the neuron than the coordinate series without jumps and this is consistent with the results exhibited in Table 3.

**Table 2** Frequency of participation in the 20 best classifications of a set of 10 relevant features. C is the number of times that each feature was ranked in the R position

| Spatial series with jumps | C | R | Spatial series without jumps | C | R |
|---|---|---|---|---|---|
| LocalMinimSDa1w1 | 22 | 1 | MeanTimSer | 24 | 1 |
| VarianceTS | 20 | 1 | KendaAutoct8 | 16 | 1 |
| MutInCEqPrb0t3 | 18 | 2 | SpearAutoct1 | 15 | 1 |
| MutInCEqPrb0t1 | 18 | 3 | PearsCAutot3 | 15 | 2 |
| KurtosisTS | 15 | 2 | SpearAutoct8 | 15 | 3 |
| DetFluctAna | 13 | 2 | LocalMinimSDa1w1 | 14 | 2 |
| PearsAutoct1 | 11 | 3 | MutInfEqPrb0t2 | 14 | 2 |
| MutInfEqDib0t3 | 8 | 1 | PearsAutoct6 | 14 | 3 |
| KendaAutoct10 | 8 | 2 | PartialAutt10 | 11 | 3 |
| MinMaxTimeMEANa1w1 | 8 | 3 | MaxMaxTimeIQRa1w1 | 9 | 2 |
| **Coordinate series with jumps** | **C** | **R** | **Coordinate series without jumps** | **C** | **R** |
| Bicorrelatt2_X | 20 | 1 | SpearCAutot2_Y | 20 | 1 |
| LocalMaximSDa1w2_Y | 20 | 1 | SpearCAutot7_X | 18 | 3 |
| AlgComEqPrb2_Z | 20 | 3 | Bicorrelatt26_Z | 17 | 1 |
| Bicorrelatt2_Z | 20 | 2 | PearsAutoct7_Z | 17 | 1 |
| LocalMaximMEDIANa1w1_X | 20 | 2 | PearsCAutot17_Y | 17 | 2 |
| Bicorrelatt7_X | 20 | 3 | SpearCAutot1_Z | 17 | 2 |
| LocalMaximMEDIANa1w1_Z | 17 | 1 | LocalMinimIQRa1w1_X | 15 | 2 |
| LocalMinimMEDIANa1w1_Z | 17 | 2 | MutInfEqPrb0t24_Z | 14 | 3 |
| MutInfEqDib0t10_Y | 14 | 3 | Bicorrelatt8_Z | 10 | 3 |
| MutInCEqPrb0t13_Y | 10 | 2 | LocalMaximSDa1w2_Y | 9 | 1 |

This table shows no coincidence for the best feature in all series, suggesting that each dataset has different properties compared to the others, and that the union set of all the features obtained from the series, can lead to improved results. Table 2 order is not a ladder because the descending sorting considers only the number C of times that the feature was ranked in the R position

**Table 3** Results of feature selection for the union of time series (*U-SERIES*). C is the number of times that each feature was ranked in the R position

| No. | Features | Type | C | R |
|---|---|---|---|---|
| 1 | PartialAutt3_X | CS-WJ | 20 | 2 |
| 2 | LocalMaximMEDIANa1w1_X | CS-WJ | 20 | 2 |
| 3 | LocalMaximSDa1w2_Y | CS-WJ | 20 | 1 |
| 4 | PartialAutt16_Y | CS-WJ | 19 | 1 |
| 5 | VarianceTS_Y | CS-WJ | 14 | 3 |
| 6 | SpearCAutot2_Y | CS-WOJ | 20 | 1 |
| 7 | PearsAutoct17_Y | CS-WOJ | 19 | 3 |
| 8 | LocalMinimSDa1w1 | SS-WJ | 20 | 3 |
| 9 | VarianceTS | SS-WJ | 19 | 2 |
| 10 | KendaCAutot1 | SS-WOJ | 10 | 1 |

This table was ordered according to the type of dataset to illustrate that *CS-WJ* exhibit five out of the ten best classifications

## Using the Union of Morphological Features and those Obtained from Series

Table 4 shows the results for the ten best ranked features. From these, three belong to the series without jumps, four to the series with jumps, and two are features from the spatial series. This result is similar to the one obtained in the previous section; however notice that in this case only three of the features were morphological. This result confirms the value of the proposed features obtained from the decomposition in 1D time series of the complex 3D neuronal trees to characterize them.

**Table 4** Results of feature selection for the union of series and morphological features (*U-MORPHO*)

| No. | Features | Type | C | R |
|---|---|---|---|---|
| 1 | SpearCAutot2_Y | CS-WOJ | 20 | 1 |
| 2 | VarianceTS | SS-WJ | 16 | 3 |
| 3 | PartialAutt3_X | CS-WJ | 14 | 2 |
| 4 | LocalMaximSDa1w2_Y | CS-WJ | 12 | 1 |
| 5 | VarianceTS_Z | CS-WOJ | 12 | 2 |
| 6 | KurtosisTS | SS-WOJ | 12 | 3 |
| **7** | **Pk_classic _Ave** | **MORPHO** | **11** | **1** |
| **8** | **Last_parent_diam** | **MORPHO** | **11** | **2** |
| 9 | VarianceTS_Y | CS-WJ | 9 | 3 |
| **10** | **Parent_Daughter_Ratio_sd** | **MORPHO** | **8** | **1** |

C is the number of times that each feature was ranked in the R position. The morphological features are highlighted in bold

## Classification

This section shows the classification results for the different neuron sets used in this work.

Table 5 exhibits the basic results of the recursive process of feature selection and classification. Classifying a dataset gives as results a total of 364 tables of this type, one per each specific evaluator - classifier combination. This table shows useful rankings that meet the 10:1 ratio of TNI (total number of instances)/FEAT (number of features), including rankings with four or fewer features. The best result of correctly classified instances (85%) was obtained with four features. The first column contains the number of features (FEAT), the second column exhibits the percentage of correctly classified instances (CCI), the third column shows the total number of instances (TNI), the fourth column the number of correctly classified instances (NCCI), the fifth column the number of incorrectly classified instances (NICI), the sixth column the area under the receiver operating characteristic (ROC) curve, and the last column the F-Measure defined in *Weka* (Bouckaert et al. 2015). The five best ranked features for this table were those numbered 4, 3 and 2, which correspond respectively, according to the *L-measure* nomenclature, were: total volume, average pathway distance, average local amplitude of bifurcations, and the standard deviation of pathway distance. Table 5 was obtained using seven evaluators, 52 classifiers, and seven cycles to select the four features and perform the classification, which generated 2548 results, 1092 of them useful because these are the ones satisfying the 10:1

**Table 5** Results of recursive selection of features and classification for the best result of correctly classified instances (CCI = 85%)

| FEAT | CCI | TNI | NCCI | NICI | ROC | F-Measure |
|---|---|---|---|---|---|---|
| 41 | 47.5 | 40 | 19 | 21 | 0.54 | 0.47 |
| 21 | 77.5 | 40 | 31 | 9 | 0.71 | 0.77 |
| 11 | 77.5 | 40 | 31 | 9 | 0.77 | 0.77 |
| 6 | 72.5 | 40 | 29 | 11 | 0.66 | 0.72 |
| **4** | **85** | **40** | **34** | **6** | **0.84** | **0.85** |
| 3 | 82.5 | 40 | 33 | 7 | 0.83 | 0.82 |
| 2 | 82.5 | 40 | 33 | 7 | 0.85 | 0.82 |

The first step in the recursive procedure is ranking the features according to their importance using the corresponding evaluator (from the seven evaluators considered) using a ranker type search algorithm. The next step is to apply recursively the ranker, leaving approximately one half of the features. For example, consider a dataset containing 40 instances and 81 features in the sequence: 41, 21, 11, 6, 4, 3 and 2. When the instances-features ratio 10:1 is fulfilled (e.g. for 4, 3 and 2 features), the classification process starts. The results are shown in this table, in which nevertheless all the classification results are included

instances-features ratio. By simplicity, we did not include in Table 5 other information as: set, evaluator, searching algorithm, classifier, classification rate (minimum, average, maximum, or standard deviation), as well as the best ranked features.

## Epilepsy Set

Figure 4 shows the box plot for the epilepsy set comparing the all classifications for each dataset of features, these corresponds to the 40 mice, 20 controls wild type mice and 20 genetically modified knock-in mice. As can be seen, the union of series features (U-SERIES), and the union of series and morphological features (U-MORPHO) were the best perform with mean classifications above 75%.

Table 6 shows the summarized results for each dataset with min, mean, max and standard deviation. Note that the mean value of all classifications using *U-SERIES* is about 72.18%, and using *CS-WJ* is less than 68%. However, the *U-MORPHO* features improved the classification reaching 95% of correct classification with a mean of 72.86%. On the other hand, *MORPHO* alone reached 87.5% of correct classification with a 67.03% mean.

Finally, the worst classifiers for this set were the *SS-WOJ* and *SS-WJ* datasets respectively. In order to determine the difference between datasets, we applied an analysis of multiple comparisons. This procedure compares two by two the results by applying the Friedman statistical test and using the Tukey's honestly significant difference criterion. This non parametric approach was selected in order to avoid making assumptions about the probability density function of the data. Figure 5 shows the difference between datasets by applying the Friedman test.

## Statistical Analysis of the Best Ranked Features

The box plot showing the best ranked morphological features for the epilepsy set is shown in Fig. 6. All the features showed significant statistical differences between them. The best correct classification percentage with these features was 87.5%, as shown in Fig. 4. Three of these morphological features showed a highly significant statistical difference ($p < 0.01$). These were: standard deviation of the contraction (*Contraction SD*), standard deviation of the angle between two branches from the father bifurcation (*Bif_amp_remote SD*), and the angle between the previous compartment of bifurcating father and the two child branches of the same bifurcation. The smaller of the two angles is returned as the result. (*Bif_tilt_local*). Also, with significant statistical difference ($p < 0.05$), there appears the standard deviation of the diameter of the first compartment after the bifurcation (*Diam_Threshold SD*).

The best result for *U-SERIES* dataset was obtained using four features (see Table 6, with 90% of success). The first feature was the linear metric Partial Autocorrelation (*PartialAut*) of "*Y*" coordinate with jumps introducing a delay of six samples. The second one was Partial Autocorrelation of "*X*" coordinates with jumps introducing a delay of three

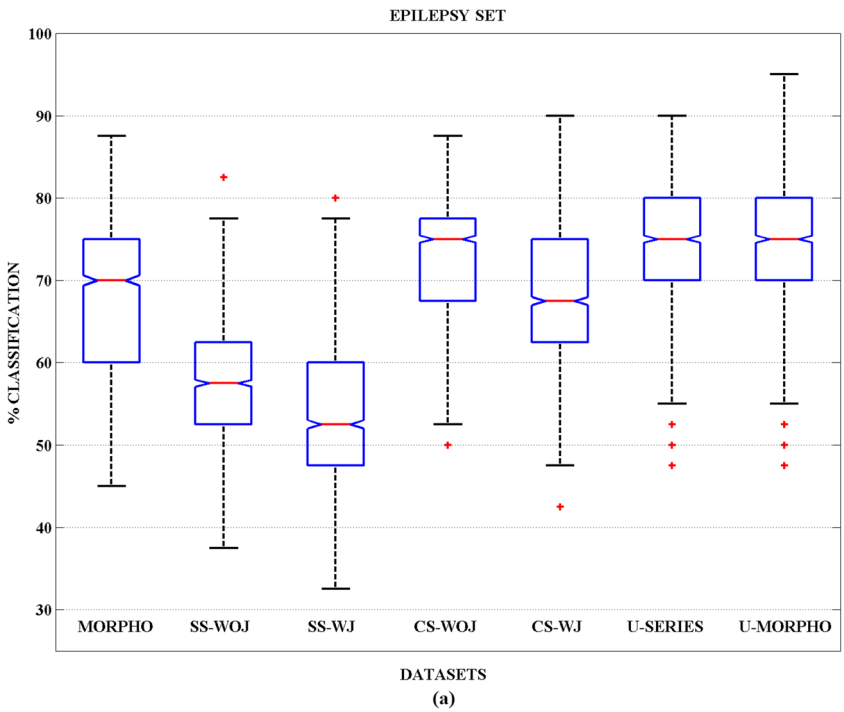


**Fig. 4** Box plot for the epilepsy set comparing all the classifications results for each dataset of features, these corresponds to the 40 mice, 20 controls *wild type mice* and 20 genetically modified *knock-in mice*. As can be seen, *CS-WOJ*, *U-SERIES* and *U-MORPHO* showed the best performance, with mean classifications above 75%

**Table 6** Comparison of all classifications results (1316) for each dataset of features from the epilepsy set

| DATASETS | MIN | MEAN | MAX | SD |
|---|---|---|---|---|
| MORPHO | 45.00 | 67.03 | 87.50 | 9.76 |
| SS-WOJ | 37.50 | 58.16 | 82.50 | 6.74 |
| SS-WJ | 32.50 | 53.90 | 80.00 | 7.95 |
| CS-WOJ | **50.00** | 70.92 | 87.50 | 9.65 |
| CS-WJ | 42.50 | 67.67 | 90.00 | 9.21 |
| U-SERIES | 47.50 | 72.18 | 90.00 | 9.89 |
| U-MORPHO | 47.50 | **72.86** | **95.00** | 10.18 |

The best outcomes are highlighted in bold

samples. The Partial Autocorrelation and other twelve metric can be computed for the given range of delays, see Appendix 1 (Online Resource 2). The 1 to 10 range was adopted as suggested by (Kugiumtzis and Tsimpiris 2010).

The second best ranked feature is the Cumulative Mutual Information (Papana and Kugiumtzis 2009) for equidistant bins (*MutInCEqDi*) for the coordinate series with jumps, which is the sum of the values of the mutual information up to the delay "*t*" (Kugiumtzis and Tsimpiris 2010), defined for the given range of delays. Partial Autocorrelation (*PartialAut*) is ranked in third place too, but with three samples of delay, whereas the mutual information of the equally-probable containers (*MutInfEqPr*) with three samples of delay occupies the fourth place (Fig. 7).

## Ischemia Set

To analyze the ischemia set we conducted the same trials previously described, having obtained the best classification (83.42% correct) with *U-MORPHO*, see Table 7. The *U-SERIES* showed a maximum of 79.90% and a mean value of 56.17%, which is lower than the mean value 59.57% obtained with the morphological features (*MORPHO*).

Table 7 shows the summarized results for each dataset with min, mean, max and standard deviation.

The comparative analysis among the various datasets used in this work revealed that the best dataset was the union of series (*U-MORPHO*) with a significant statistical difference in comparison to the other datasets, see in (Online Resource 7, Fig. 1) shown in (a) the % of right classification for each feature dataset using the ischemia set, in (b) multiple comparisons using the Friedman test.

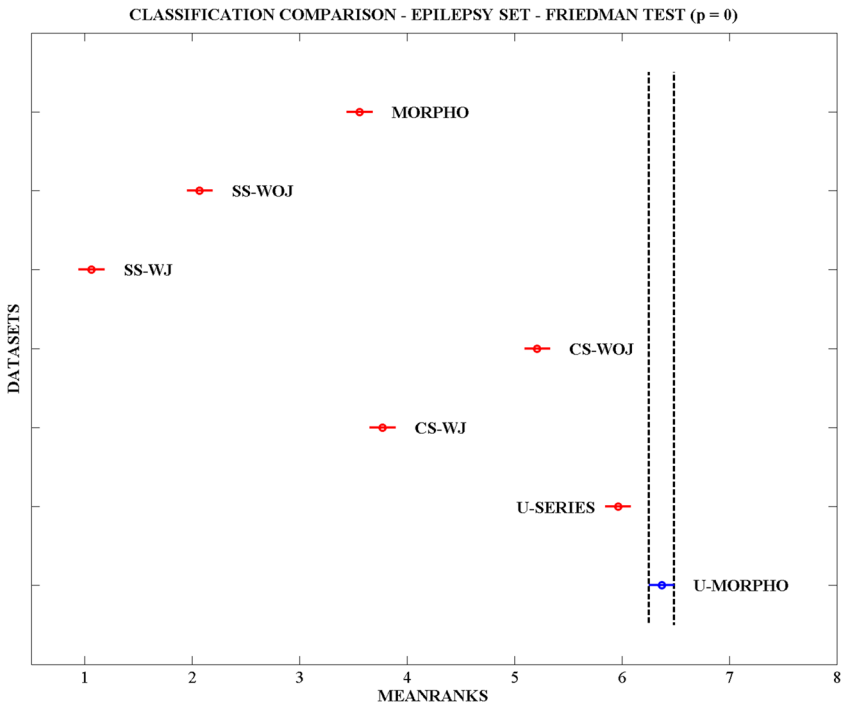


**Fig. 5** The graph shows the best datasets of features obtained by multiple comparisons using the Friedman test. The *U-MORPHO* dataset showed a significant statistical difference when compared with the remaining datasets. The remaining sets behave similarly with the exception of *MORPHO* and *CS-WJ* which do not show statistically significant differences between them. This result is due to the wide dispersion of the classification results around the mean value and to the large number of values compared: 9212 in total and 1316 for each dataset. This figure shows also that the results from the coordinate series are better than those from the spatial series. It is observed also that *U-SERIES* improved the results obtained with each one of the coordinate series taken independently. The x-axis label contains information about which mean ranks are significantly different from the selected mean ranks. In Fig. 4 *U-MORPHO* (in blue), is significantly different from the rest of the dataset (in red)

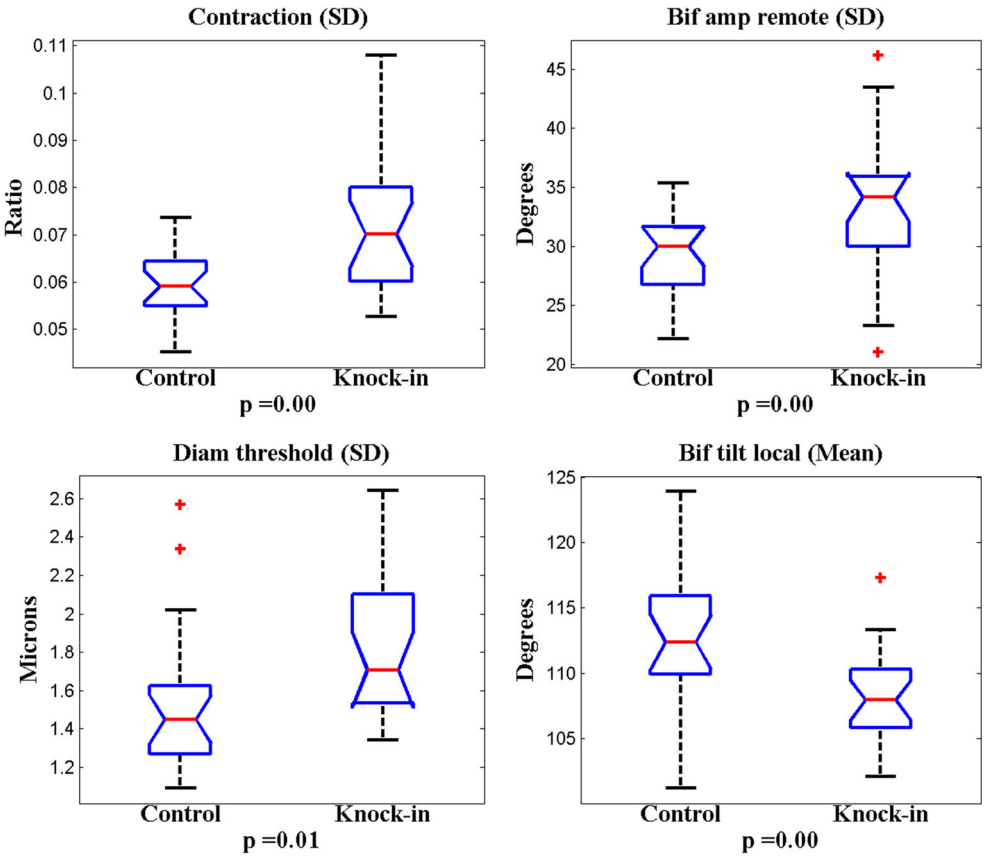


**Fig. 6** Box plot of the four best ranked morphological features obtained using *L-measure* in a set of 40 mice, 20 controls (wild type mice) and 20 genetically modified (knock-in mice)

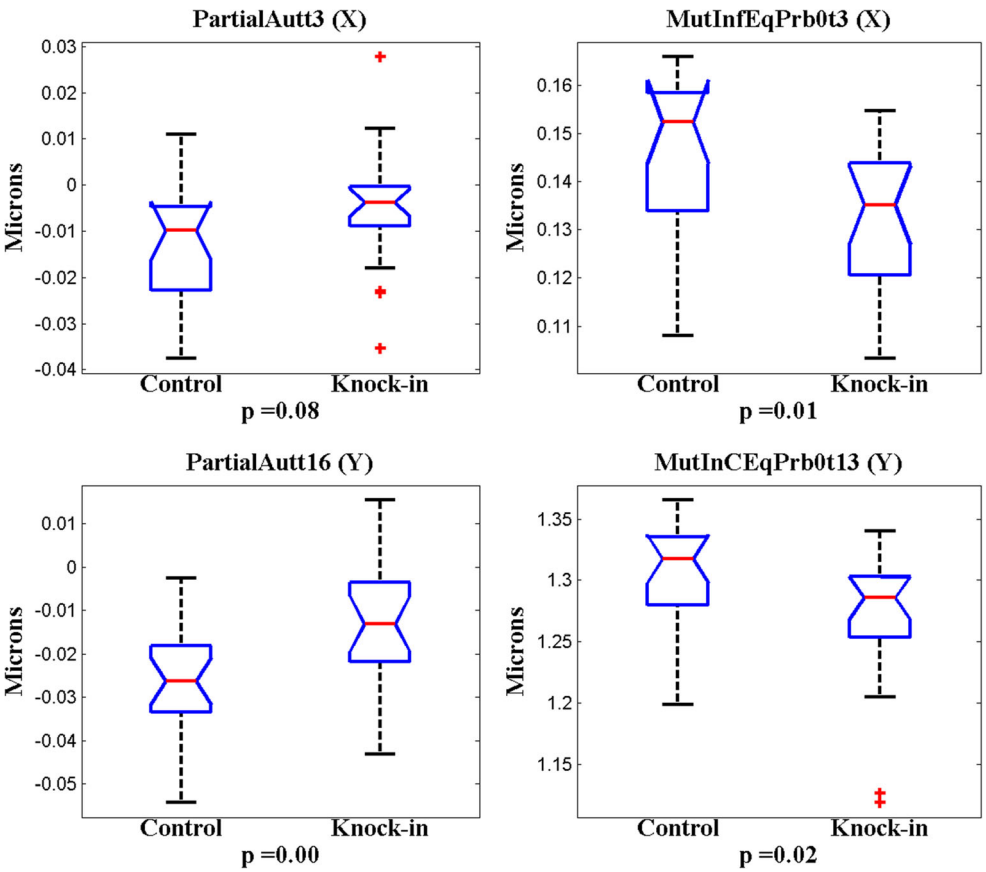


**Fig. 7** Box plot of the four best ranked *U-SERIES* features obtained using *MATS* in epilepsy set with 40 mice, 20 controls (wild type mice) and 20 genetically modified (knock-in mice)

**Table 7** Comparison among all classifications for each dataset of features from the ischemia set

| DATASETS | MIN | MEAN | MAX | SD |
|---|---|---|---|---|
| MORPHO | **49.25** | 59.57 | 69.85 | 4.16 |
| SS-WOJ | 44.22 | 55.18 | 69.85 | 3.82 |
| SS-WJ | 43.22 | 53.35 | 70.35 | 4.36 |
| CS-WOJ | 42.71 | 56.52 | 78.89 | 5.07 |
| CS-WJ | 41.21 | 55.18 | 73.37 | 4.84 |
| U-SERIES | 41.21 | 56.17 | 79.90 | 6.65 |
| U-MORPHO | 46.73 | **60.54** | **83.42** | 5.71 |

The best results are highlighted in bold. For this set, dataset *MORPHO* shows better results than all the series-based datasets, including *U-SERIES*. The contribution of the features obtained by means of the algorithm proposed in this work can be appreciated in the *U-MORPHO* dataset result, which increases the mean CCR (correct classification rate) up to 60.54% and the maximum to 83.42%. This table shows also that the maximum values obtained by the datasets. *SS-WJ, CS-WOJ, CS-WJ and U-SERIES* are higher than the best results reached by the dataset *MORPHO*

**Table 8** Comparison of all classifications for each dataset of features from Alzheimer's disease (long projection) set

| DATASET | MIN | MEAN | MAX | SD |
|---|---|---|---|---|
| MORPHO | 41.86 | 63.64 | 79.07 | 7.39 |
| SS-WOJ | 32.56 | 54.43 | 86.05 | 8.82 |
| SS-WJ | 39.53 | 57.04 | 88.37 | 6.95 |
| CS-WOJ | **44.19** | **67.39** | 83.72 | 6.88 |
| CS-WJ | 51.16 | 67.09 | 90.70 | 7.43 |
| U-SERIES | 41.86 | 61.89 | 86.05 | 7.64 |
| U-MORPHO | 41.86 | 63.70 | **93.02** | 9.27 |

The best results are highlighted in bold. This table shows the summarized results for each dataset with min, mean, max and standard deviation. The best mean results are obtained with *CS-WOJ and CS-WJ* without large differences in the standard deviations for these sets. There exist, however, large differences in the maximum values of the results, which suggests that there are classifiers which using the proposed features can reach better results than using morphometric features, as for example occurs with dataset *CS-WJ*

Figure 2 in Online Resource 7 shows (a) the box plot of the four best ranked morphological features and (b) the box plot of the four best ranked features obtained using *MATS* in the ischemia set. The best features for this ischemia set were: *LocalMaximSDa1w2* (standard deviation of the local maximum in the "*Y*" series with jumps) *LocalMaximMEDIANa1w1* (median of the local maximum from the "*X*" series with jumps) *LocalMinimSDa1w1* (standard deviation of the local minimum from the spatial series with jumps) *Bicorrelatt9* (bi-correlation with a delay of "*9*" samples from the spatial series with jumps). The three first in this list reached statistical significances $p < 0.01$, and the last $p < 0.05$. On the other hand, the best ranked morphological features were: *Diam Threshold* (average), *Bif torque local* (average), *Last Parent Diam* (average) and *Heigth* (average). Among them, the first three showed high significant statistical difference $p < 0.01$, and the other one had significant statistical difference $p < 0.05$ between the control and ischemia sets. Notice that only the best four features from each dataset were analyzed here; Notice also that the best classification of the *U-SERIES* dataset was obtained using 17 features, and from the *MORPHO* dataset with only three features. The other feature mentioned above (Last Parent Diam) corresponds to the second best classification.

## Alzheimer's Disease Set

These sets of neurons comprised two subsets, corresponding to long projections neurons and local projection neurons. Table 8 shows the summarized results for each dataset with min, mean, max and standard deviation. The best classification for the long projection neurons was obtained with the dataset of *CS-WOJ*, which classified correctly 67.39% of the instances in the mean. It can be seen also in Table 8 that the correct classification ranged from 44.19 to 83.72%. The *U-MORPHO* dataset obtained a maximum of 93.02% CCR, whereas the *U-SERIES* only reached a maximum of 86.05% which is similar to the maximum of *SS-WOJ* dataset. In this case, datasets *SS-WOJ and SS-WJ* showed the worst performance.

Morphological features exhibited the maximum worst performance for this dataset (*MORPHO*), with 79.07% of highest success, while the mean and minimum values of the MORPHO dataset were higher than the corresponding values for the *SS-WOJ* and *SS-WJ* datasets. Generally speaking, in all the studied sets the *MORPHO* dataset showed a better performance than the sets based in spatial series. See Fig. 3 in Online Resource 7 showing in (a) the percentage of correct classification for each feature dataset using the Alzheimer's disease (long projection) set and in (b) multiple comparisons using the Friedman test.

Figure 4 (Online Resource 7) shows the details of the four best features obtained with *MORPHO* and *CS-WJ* datasets: (a) the box plot of the four best ranked morphological features and (b) the box plot of the best ranked features obtained using *MATS*.

In (Kabaso et al. 2009) the authors analyze a different set of neurons to study the Alzheimer's disease (local projection neurons). They used four metrics to characterize the apical and basal trees (dendritic volume, total dendritic length, total dendritic surface area, and apical trunk diameter). According to these features, these datasets did not show significant statistical differences between them. The study presented in this work compared the morphological features obtained from *L-measure* with those from the time

series. Using morphological features we obtained 86.49% of correct classification, whereas using *CS-WOJ* dataset resulted in 89.19%. Table 9 shows the summarized results for each dataset with min, mean, max and standard deviation. See in Fig. 5 Online Resource 7 shows in (a) the % of correct classification for each feature dataset using the Alzheimer's disease (local projection) set and in (b) multiple comparisons using the Friedman test.

These results confirm the improvement in classification using the features proposed in this work. None of the classifiers using each dataset separately outperformed 92% of correct classification; however, grouping the best features of each dataset, including the morphological one, allowed 97.30% of correct classification rate. Figure 6 (Online Resource 7) exhibits the details of the four best features obtained with morphological and *CS-WOJ* dataset: (a) the box plot of the best ranked morphological features and (b) the box plot of the four best ranked features obtained using *MATS*.

## Alternative Method Using Training and Test Set

The results of this process are shown in detail in Online Resource 4. As can be observed, there is not a large difference when the new results are compared to the previous ones and moreover these new results support the usefulness of the proposed new features in comparison to using only the conventional ones. In particular the main issues obtained for this same Epilepsy set are preserved (see Figs. 1 and 2 of the Online Resource 4 and compare with Figs. 4 and 5 in this paper), these are:

**Table 9** Comparison of all classifications for each dataset of features from Alzheimer's disease (local projection) set in terms of CCR

| DATASETS | MIN | MEAN | MAX | SD |
|---|---|---|---|---|
| MORPHO | **45.95** | 65.57 | 86.49 | 7.22 |
| SS-WOJ | 43.24 | 70.90 | 86.49 | 9.01 |
| SS-WJ | 37.84 | 55.59 | 86.49 | 8.52 |
| CS-WOJ | 43.24 | 66.57 | 89.19 | 7.69 |
| CS-WJ | 35.14 | 65.06 | 86.49 | 9.42 |
| U-SERIES | 43.24 | 68.56 | 86.49 | 10.17 |
| U-MORPHO | **45.95** | **72.81** | **97.30** | 12.17 |

The best results are highlighted in bold. In terms of mean values, the best results are reached for dataset *U-MORPHO* with 72.81% followed by *SS-WOJ* with 70.90%, the latter is a result which did not behave in similar way than the rest of the analyzed datasets. Its similar *SS-WJ* showed the worst performance with 55.59%. In regard to the maximum values there are five datasets that share the same value with 86.49% only surpassed by *CS-WOJ and U-MORPHO* with 89.19 and 97.30% respectively; *U-MORPHO* showed the best results (minimum, mean and maximum) which supports using the union of all features to improve the classification results

- Classification with the coordinate series showed a better performance than with the spatial series.
- The classification results were improved when using the union of features *U-SERIES* and *U-MORPHO*.
- The morphological features showed a better performance than the spatial series and behaved worse when compared to the rest of the datasets.

Some differences among the results can be also observed. These are:

- With the alternative method, six out of seven datasets reached at least one classification with all cases correctly classified.
- The dispersion of the correct classification rate results is smaller for the first procedure used in this research, and the mean values are inferior in more than 10% for the alternative method employed later.

Tables 1 and 2 in Online Resource 4 show that in both cases the U-MORPHO and U-SERIES datasets improve the results obtained with the MORPHO dataset in approximately 5%. This is also the case for the CS-WOJ and CS-WJ datasets with values that ranged between 0.6% and 3.8%. Using any of the two procedures it was shown that decomposing appropriately the three-dimensional structure of the neuron into time series, allowed obtaining features which led to a better description of the neuronal morphology to the effects of neuron classification. Moreover, there was not found a large difference when the new results are compared to the previous ones, and this tends to support the usefulness of the proposed new features in comparison to using only the already known conventional ones.

## Area under ROC Curve

The area under the ROC curve was estimated for each classification, but as the total amount of classifications is very high for the whole results, it is difficult to represent all these area under ROC values. Trying to overcome this limitation, these results are presented by means of box plots as was done for the classifications. In the Online Resource 8 the ROC areas box plots are shown for each of the studied sets.

## Evaluators and Classifiers

The whole results comprised 28 different datasets and were analyzed using the statistical evaluation of multiple algorithms in multiple problems, described in (Demšar 2006) and implemented in (Calvo and Santafe 2015). This allowed determining which evaluators and classifiers exhibited the best performance. The relationship among the implemented evaluators is shown in Fig. 8. Here the analysis took into account all scores

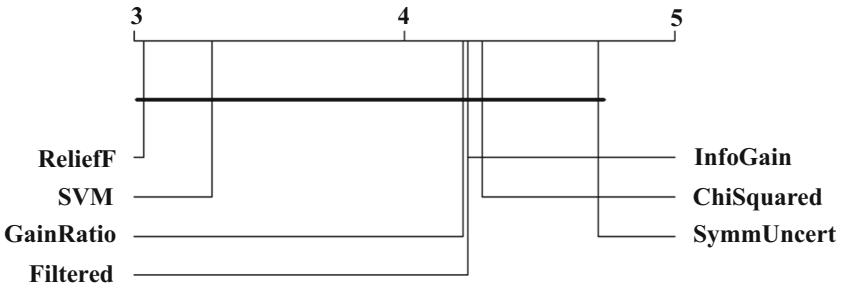


**Fig. 8** Comparison of evaluators using post hoc tests for multiple comparison analyses, represented by means of a critical difference plot which contains the average ranks of each one of the various methods. This result was obtained using the critical difference plot with corrected p-value. The top line in the diagram is the axis on which was plotted the critical difference which contains the average ranks of methods (Demšar 2006). Those algorithms that showed no significant differences among them appear grouped together using a bold horizontal line

obtained by each dataset. As it can be seen, the evaluator of features based on *ReliefF* showed the best average rank. However, this analysis did not show statistically significant differences among the seven evaluators that were compared. Figure 8 was obtained using the critical difference plot with corrected *p*-value. The top line in the diagram is the axis on which was plotted the critical difference plot which contains the average ranks of methods (Demšar 2006). Those algorithms that showed no significant differences among them appear grouped together by means of a bold horizontal line.

The analysis for the best nine classifiers is shown in Fig. 9. There are no significant statistical differences among them.. This results agrees with those in (Guerra et al. 2011) which asserts that it is probable that the precision in results is not related to the classification algorithm employed.

## Discussion

The goal of this research has been to propose new features for neuron classification and validate their effectiveness when classifying dendritic structures with high morphological complexity. To accomplish this, three pathologically affected neuron groups were classified using the results of this methodology.

We explored the variability of the main branches and branch segments associated to them along their path from the root until the terminations, by means of the features obtained from time series. This method analyzes the dendrite considering the contribution of each one of its constituent elements. Time series analysis allows obtaining a great variety of features in a unique structure which describes the high neuronal tree complexity. On the other hand, it includes the nonlinear analysis which has demonstrated to be a powerful tool to quantify the complexity of spatial structures with irregular forms (Di Ieva et al. 2015). It is very unlikely that two series coming from different morphological structures might have similar features.

The morphological method is based in the analysis of elementary statistics like minimum, maximum, mean, standard deviation and counting of instances. This method might be less efficient when dealing with spatial properties. With this method, the metrics are usually calculated from the measurements in each traced segment. The results are then added or averaged to obtain a representative value for the neuronal tree, for example volume, area, length etc. that might be similar in trees with different morphology.

### Epileptic Disorders can Be Evaluated Using Neuronal Time Series Features

In (Beguin et al. 2013) it has been disclosed that the mutation of gen *ARX(GCG)7* has no effect over the interneuron dendritic arborization. Conversely, the axonal arborization in pyramidal cells of *ARX(GCG)7* modified mice is abnormal, and can show a neuronal reorganization which contribute to the appearance of epilepsy. Additionally, (Ascoli et al. 2007)

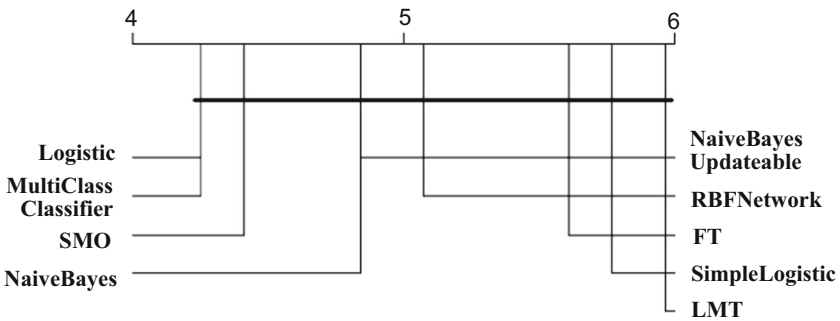


**Fig. 9** Comparison of classifier algorithms using post hoc tests for multiple comparison analyses and represented with a critical difference plot containing the average ranks of methods. The best 6 classifiers are including in Bayes and Function groups defined by *Weka*

offers 40 digitally reconstructed neurons divided in 20 from genetically modified mice *knock-in mice* with the mutation *ARX(GCG)7* using the procedure reported in (Beguin et al. 2013), and 20 from unmodified *wild type mice*.

Our method has been used to verify the pathological significance of mutation *ARX(GCG)7* using the whole neuronal tree, that is, without partitioning it into dendritic and axonal trees. Supervised classification results showed that there are features from the time series which can allow classifying correctly 72.18% of digitally reconstructed neurons. Conversely, using morphological features the best result only reached 67.03%, the same result as that obtained by (Beguin et al. 2013). This 5.15% improvement in classification supports the usefulness of the proposed features from the time series. All the classifications percentages mentioned above correspond to mean values.

### The Reduction in the Complexity of Neuronal Structures Caused by Alzheimer's Disease can Be Established by the Proposed Procedure

According to (Duan et al. 2003) in which the results were obtained through Sholl analysis, there are significant differences due to aging in the reduction of the number of spines and their density in apical and basal dendritic trees. Also, they conclude that changes in the dendritic structure can only be observed in a portion of apical dendrites.

Using our procedure we obtained that there are also differences between both apical and basal dendritic trees, and these differences can be detected using features obtained by the analysis of the time series. Moreover, using the new features the effectiveness in classification reached a maximum of 90.7% with a mean value of correct classification rate of 67.39%, whereas using only the morphological features obtained by (Scorcioni et al. 2008) this was only 79.07 and 63.64% maximum and mean values respectively. The best ranked feature in this trial was: Spearman cumulative autocorrelation. The effectiveness of the proposed procedure has been based on the linear and nonlinear analysis of time series obtained from highly complex morphological structures stated by (Papana and Kugiumtzis 2009). This result also suggests that the proposed procedure can be useful to analyze the Alzheimer's disease's pathology, in which the complexity of neuron structures decreases.

### The New Features might Improve Ischemia Classification

The authors of (Dean et al. 2013) compare a set of one hundred control neurons and a hundred ischemic neurons to test if the impaired cortical growing is related to deficits in dendritic arbor maturation. For this purpose, Golgi-impregnated neurons were constructed four weeks after ischemia and it was determined whether the reduction in cortical volume at this time was associated with disturbances in maturation of the basal dendritic arbor of pyramidal neurons. The results of this comparison showed that pyramidal neurons suffer a significant reduction in: the number of basal dendritic branches in about an 18%, and the number of basal nodes in about 24%. In the Sholl analysis the ischemia group displayed an overall reduction in the number of dendritic intersections (*ANOVA,* $p < 0.0001$), with the most significant differences observed at 25 to 75 μm from the cell soma.

Our results, obtained from the supervised comparison of whole dendritic trees, were capable of correctly classify around 79.90% of the neurons in their corresponding groups. Despite this relative low rate of success, the obtained results outperformed those obtained using solely morphological features under the same conditions, which showed only 69.85% of effectiveness, for a difference of 10.05%. The above mentioned values are referred to maximum values. In term of mean values the morphometric features outperformed the time series features dataset with 59.57% CCR, see Table 7. This result could lead to interpretation errors due to the use of all classification results. When comparing the results of the 20 best classifications using boxplot (Fig. 2(a) Online Resource 5) with all classification results boxplot (Fig. 1(a) Online Resource 5), we can see the differences. The low classification rate obtained using our method was probably related to the fact that the whole dendritic tree was used to detect changes in only a small part of it (basal dendrites); however, the goal was only to support the usefulness of the novel features in the classification task for ischemic neurons. There is an agreement between the results of the statistical comparison and the results of classification. The features obtained from time series showed larger significant statistical differences than those using the morphological features, as well as a higher CCR. However, the best ranked feature in the morphological dataset (*average Hillman threshold*) did not show significant statistical differences for its values between the ischemia and control groups. Despite this, the mentioned feature showed to bring useful information that improved the classification when used together with other features.

## Conclusion

In this paper, we developed a new method to obtain neuron features, based in the concept of topological equivalency, and decomposed the 3D structure of the reconstructed neuronal tree into time series. Using the *MATS* tool, a broad set of features was extracted from each time series. We made use of the *Weka* tool to select the features obtained and to evaluate their effectiveness during classification of neurons. The experimental results demonstrated the capability of the proposed method to obtain improvements in classification in terms of CCR, using the features proposed in this work. These results

were: 5.15, 3.75, 5.33% for epilepsy and Alzheimer's disease (long and local projections) respectively. Using the all classifications' results for the ischemia set, the morphological features dataset was better than the time series datasets, with 3.05% CCR. The following issues are left as proposals for future work: Applying the proposed method to each dendritic path to obtain the proposed features and analyzing the differences between classifications using manually and automated traced neurons as well as the influence of reconstruction errors on the quality of classification.

## Information Sharing Statement

The reconstructed neurons used in this paper are available at NeuroMorpho.Org (RRID:SCR_002145) inventory:

http://neuromorpho.org/NeuroMorpho_Linkout.jsp?PMID=12902394 (Alzheimer disease sets).

http://neuromorpho.org/NeuroMorpho_Linkout.jsp?PMID=23325800 (Ischemia set).

http://neuromorpho.org/NeuroMorpho_Linkout.jsp?PMID=22628459 (Epilepsy set).

All software used were freeware: The *MATS* toolbox available at https://arxiv.org/abs/1002.1940, Weka (RRID:SCR_001214) available at http://www.cs.waikato.ac.nz/ml/weka/ and *L-measure (RRID:SCR_003487)*, available at http://cng.gmu.edu:8080/Lm/.

**Acknowledgments** The authors wish to thank the NeuroMorpho.Org project and Dr. Giorgio Ascoli for providing the information on traced neurons as well as statistical data used in this research for comparison purposes. We also acknowledge Drs. Carlos Morell-Pérez and María M. García-Lorenzo and BSc. José D. López-Cabrera for their useful comments and having providing useful references, as well as to the anonymous reviewers for their criticism and valuable comments that allowed us to introduce many improvements in the article.

## Compliance with Ethical Standards

**Conflict of Interest** All the authors declare no conflicts of interest.

## References

*0 - 1 test for chaos - File Exchange - MATLAB Central*. (2018). https://www.mathworks.com/matlabcentral/fileexchange/25050-0-1-test-for-chaos.

Absoud, M., Parr, J. R., Halliday, D., Pretorius, P., Zaiwalla, Z., & Jayawant, S. (2010). A novel ARX phenotype: rapid neurodegeneration with Ohtahara syndrome and a dyskinetic movement disorder. *Dev Med Child Neurol, 52*(3), 305–307. https://doi.org/10.1111/j.1469-8749.2009.03470.x.

Alligood, K. T., Sauer, T. D., & Yorke, J. A. (2009). *Chaos: An introduction to dynamical systems (Corrected edition.)*. New York: Springer.

Armañanzas, R., & Ascoli, G. A. (2015). Towards automatic classification of neurons. *Trends Neurosci, 38*(5), 307–318. https://doi.org/10.1016/j.tins.2015.02.004.

Ascoli, G. A., Donohue, D. E., & Halavi, M. (2007). NeuroMorpho.Org: a central resource for neuronal morphologies. *J Neurosci, 27*(35), 9247–9251. https://doi.org/10.1523/JNEUROSCI.2055-07.2007.

Backes, A. R., & Bruno, O. M. (2012). Fractal and Multi-Scale Fractal Dimension analysis: a comparative study of Bouligand-Minkowski method. *arXiv:1201.3153 [cs]*. http://arxiv.org/abs/1201.3153. Accessed May 23, 2014.

Beguin, S., Crépel, V., Anikstejn, L., Becq, H., Pelosi, B., Pallesi-Pocachard, E., Bouamrane, L., Pasqualetti, M., Kitamura, K., Cardoso, C., & Represa, A. (2013). An epilepsy-related ARX polyalanine expansion modifies glutamatergic neurons excitability and morphology without affecting GABAergic neurons development. *Cerebral Cortex (New York, NY: 1991), 23*(6), 1484–1494. https://doi.org/10.1093/cercor/bhs138.

BenSaïda, A. (2015). A practical test for noisy chaotic dynamics. *SoftwareX, 3-4*, 1–5. https://doi.org/10.1016/j.softx.2015.08.002.

Bianchi, S., Stimpson, D. C., Bauernfeind, A., Schapiro, S., Baze, W., Mcarthur, M., et al. (2012). Dendritic morphology of pyramidal neurons in the chimpanzee neocortex: regional specializations and comparison to humans. *Cerebral Cortex (New York, NY: 1991), 23*, 2429–2436. https://doi.org/10.1093/cercor/bhs239.

Bouckaert, R., Frank, E., Hall, M., Kirkby, R., Reutemann, P., Seewald, A., & Scuse, D. (2015). *WEKA manual for version 3–6-13*. CreateSpace Independent Publishing Platform.

Calvo, B., & Santafe, G. (2015). *scmamp: Statistical comparison of multiple algorithms in multiple problems*. https://cran.r-project.org/web/packages/scmamp/index.html. Accessed October 17, 2016.

Chaos and Time-Series Analysis. (2018, enero 17). http://sprott.physics.wisc.edu/chaostsa/. Accessed January 17, 2018.

Cross, S. S. (1994). The application of fractal geometric analysis to microscopic images. *Micron, 25*(1), 101–113. https://doi.org/10.1016/0968-4328(94)90057-4.

Cuntz, H., Forstner, F., Borst, A., & Häusser, M. (2011). The TREES toolbox–probing the basis of axonal and dendritic branching. *Neuroinformatics, 9*(1), 91–96. https://doi.org/10.1007/s12021-010-9093-7.

Dean, J. M., McClendon, E., Hansen, K., Azimi-Zonooz, A., Chen, K., Riddle, A., Gong, X., Sharifnia, E., Hagen, M., Ahmad, T., Leigland, L. A., Hohimer, A. R., Kroenke, C. D., & Back, S. A. (2013). Prenatal cerebral ischemia disrupts MRI-defined cortical microstructure through disturbances in neuronal arborization. *Sci Transl Med, 5*(168), 168ra7. https://doi.org/10.1126/scitranslmed.3004669.

Delgado Castillo, D., Martín Pérez, R., Hernández Pérez, L., Orozco Morález, R., & Lorenzo Ginori, J. (2016). Algoritmos de aprendizaje automático para la clasificación de neuronas piramidales afectadas por el envejecimiento. *Revista Cubana de Informática Médica, 8*, 559–571.

Demšar, J. (2006). Statistical comparisons of classifiers over multiple data sets. *J Mach Learn Res, 7*(Jan), 1–30.

Di Ieva, A., Grizzi, F., Jelinek, H., Pellionisz, A. J., & Losa, G. A. (2013). Fractals in the neurosciences, part I: general principles and basic neurosciences. *The Neuroscientist: A Review Journal Bringing Neurobiology, Neurology and Psychiatry, 20*(4), 403–417. https://doi.org/10.1177/1073858413513927.

Di Ieva, A., Esteban, F. J., Grizzi, F., Klonowski, W., & Martín-Landrove, M. (2015). Fractals in the neurosciences, part II: clinical applications and future perspectives. *The Neuroscientist: A Review Journal Bringing Neurobiology, Neurology and Psychiatry, 21*(1), 30–43. https://doi.org/10.1177/1073858413513928.

Dokukin, M. E., Guz, N. V., Gaikwad, R. M., Woodworth, C. D., & Sokolov, I. (2011). Cell surface as a fractal: normal and cancerous cervical cells demonstrate different fractal behavior of surface adhesion maps at the nanoscale. *Phys Rev Lett, 107*(2), 028101. https://doi.org/10.1103/PhysRevLett.107.028101.

Duan, H., Wearne, S. L., Morrison, J. H., & Hof, P. R. (2002). Quantitative analysis of the dendritic morphology of corticocortical projection neurons in the macaque monkey association cortex. *Neuroscience, 114*(2), 349–359.

Duan, H., Wearne, S. L., Rocher, A. B., Macedo, A., Morrison, J. H., & Hof, P. R. (2003). Age-related dendritic and spine changes in corticocortically projecting neurons in macaque monkeys. *Cerebral Cortex (New York, N.Y.: 1991), 13*(9), 950–961.

Fernández, E., & Jelinek, H. F. (2001). Use of fractal theory in neuroscience: methods, advantages, and potential problems. *Methods (San Diego, Calif.), 24*(4), 309–321. https://doi.org/10.1006/meth.2001.1201.

Foster, K. R., Koprowski, R., & Skufca, J. D. (2014). Machine learning, medical diagnosis, and biomedical engineering research - commentary. *Biomed Eng Online, 13*, 94. https://doi.org/10.1186/1475-925X-13-94.

Gottwald, G. A., & Melbourne, I. (2009). On the implementation of the 0-1 test for chaos. *SIAM J Appl Dyn Syst, 8*(1), 129–145. https://doi.org/10.1137/080718851.

Gottwald, G. A., & Melbourne, I. (2016). The 0-1 test for Chaos: a review. *SpringerLink*, 221–247. https://doi.org/10.1007/978-3-662-48410-4_7.

Guerra, L., McGarry, L. M., Robles, V., Bielza, C., Larrañaga, P., & Yuste, R. (2011). Comparison between supervised and unsupervised classifications of neuronal cell types: a case study. *Developmental Neurobiology, 71*(1), 71–82. https://doi.org/10.1002/dneu.20809.

Halavi, M., Hamilton, K. A., Parekh, R., & Ascoli, G. A. (2012). Digital reconstructions of neuronal morphology: three decades of research trends. *Front Neurosci, 6*. https://doi.org/10.3389/fnins.2012.00049.

Hamilton, P., & West, B. (2000). Software review chaos data analyzer, professional version. by J. Sprott and G. Rowlands. *Nonlinear Dynamics, Psychology, and Life Sciences, 4*, 195–199. https://doi.org/10.1023/A:1009580513427.

Kabaso, D., Coskren, P.J., Henry, B.I., Hof, P.R., & Wearne, S.L. (2009). The electrotonic structure of pyramidal neurons contributing to prefrontal cortical circuits in macaque monkeys is significantly altered in aging. *Oxford University Press, 19*, 2248–2268. https://doi.org/10.1093/cercor/bhn242.

Kugiumtzis, D., & Tsimpiris, A. (2010). Measures of analysis of time series (MATS): a MATLAB toolkit for computation of multiple measures on time series data bases. *arXiv:1002.1940 [stat]*. http://arxiv.org/abs/1002.1940. Accessed February 27, 2018.

Leite-Morris, K. A., Kobrin, K. L., Guy, M. D., Young, A. J., Heinrichs, S. C., & Kaplan, G. B. (2014). Extinction of opiate reward reduces dendritic arborization and c-Fos expression in the nucleus accumbens core. *Behav Brain Res, 263*, 51–59. https://doi.org/10.1016/j.bbr.2013.12.041.

Mavroudis, I. A., Manani, M. G., Petrides, F., Petsoglou, C., Njau, S. N., Costa, V. G., & Baloyannis, S. J. (2014). Dendritic and spinal alterations of neurons from Edinger-Westphal nucleus in Alzheimer's disease. *Folia Neuropathol, 52*(2), 197–204.

NeuroMorpho_Linkout. (2018, febrero 28). http://neuromorpho.org/NeuroMorpho_Linkout.jsp?PMID=12902394. Accessed February 28, 2018.

Papana, A., & Kugiumtzis, D. (2009). Evaluation of mutual information estimators for time series. *International Journal of Bifurcation and Chaos, 19*(12), 4197–4215. https://doi.org/10.1142/S0218127409025298.

Pawel, S., Frishman, D., & Kramer, S. (2009). Pitfalls of supervised feature selection. *Bioinformatics (Oxford, England), 26*, 440–443. https://doi.org/10.1093/bioinformatics/btp621.

Rand, D., & Young, L.-S. (Eds.). (1981). *Dynamical systems and turbulence, Warwick 1980* (Vol. 898). Berlin, Heidelberg: Springer Berlin Heidelberg. https://doi.org/10.1007/BFb0091903

Riddle, A., Luo, N. L., Manese, M., Beardsley, D. J., Green, L., Rorvik, D. A., Kelly, K. A., Barlow, C. H., Kelly, J. J., Hohimer, A. R., & Back, S. A. (2006). Spatial heterogeneity in oligodendrocyte lineage maturation and not cerebral blood flow predicts fetal ovine periventricular white matter injury. *J Neurosci, 26*(11), 3045–3055. https://doi.org/10.1523/JNEUROSCI.5200-05.2006.

Riddle, A., Dean, J., Buser, J. R., Gong, X., Maire, J., Chen, K., Ahmad, T., Cai, V., Nguyen, T., Kroenke, C. D., Hohimer, A. R., & Back, S. A. (2011). Histopathological correlates of magnetic resonance imaging-defined chronic perinatal white matter injury. *Ann Neurol, 70*(3), 493–507. https://doi.org/10.1002/ana.22501.

Rosenstein, M. T., Collins, J. J., & Luca, C. J. D. (1993). A practical method for calculating largest Lyapunov exponents from small data sets. *Physica D, 65*, 117–134.

Saeb, T., & Hövel, P. (2013). *Dynamical systems in neuroscience*. Institut für Theoretische Physik, Technische Universität Berlin. http://www.itp.tu-berlin.de/fileadmin/a3233_bccn-nachwuchsgruppe/dynamical_systems.pdf.

Schierwagen, A., Costa, L. da F., Alpár, A., & Gärtner, U. (2007). Multiscale fractal analysis of cortical pyramidal neurons. En A. Horsch, T. M. Deserno, H. Handels, H.-P. Meinzer, & T. Tolxdorff (Eds.), *Bildverarbeitung für die Medizin 2007* (pp. 424–428). Springer Berlin Heidelberg. http://link.springer.com/chapter/10.1007/978-3-540-71091-2_85. Accessed may 22, 2014.

Schierwagen, A., Costa, L. da F., Alpar, A., Gärtner, U., & Arendt, T. (2008). Neuromorphological phenotyping in transgenic mice: a multiscale fractal analysis. En A. Deutsch, R. B. de la Parra, R. J. de Boer, O. Diekmann, P. Jagers, E. Kisdi, et al. (Eds.), *Mathematical Modeling of Biological Systems, Volume II* (pp. 185–192). Birkhäuser Boston. http://link.springer.com/chapter/10.1007/978-0-8176-4556-4_16. Accessed may 22, 2014.

Scorcioni, R., Polavaram, S., & Ascoli, G. A. (2008). L-measure: a web-accessible tool for the analysis, comparison and search of digital reconstructions of neuronal morphologies. *Nat Protoc, 3*(5), 866–876. https://doi.org/10.1038/nprot.2008.51.

Sholl, D. A. (1953). Dendritic organization in the neurons of the visual and motor cortices of the cat. J Anat, 87(4), 387-406.

Task Force of the European Society of Cardiology and the North American Society of Pacing and Electrophysiology. (1996). Heart rate variability: standards of measurement, physiological interpretation and clinical use. *Circulation, 93*(5), 1043–1065.

TISEAN: Nonlinear Time Series Analysis. (2018, enero 17). https://www.pks.mpg.de/~tisean/. Accessed January 17, 2018.

Vasilkoski, Z., & Stepanyants, A. (2009). Detection of the optimal neuron traces in confocal microscopy images. *J Neurosci Methods, 178*(1), 197–204. https://doi.org/10.1016/j.jneumeth.2008.11.008.

Wallis, J. W., & Miller, T. R. (1991). Three-dimensional display in nuclear medicine and radiology. *J Nucl Med, 32*(3), 534–546.

Zhou, Z., Liu, X., Long, B., & Peng, H. (2016). TReMAP: automatic 3D neuron reconstruction based on tracing, reverse mapping and assembling of 2D projections. *Neuroinformatics, 14*(1), 41–50. https://doi.org/10.1007/s12021-015-9278-1.